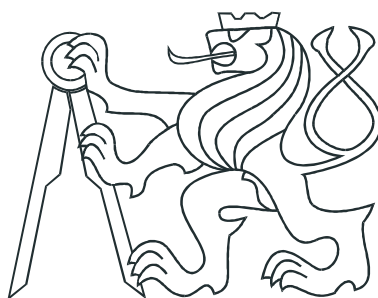


**CZECH TECHNICAL UNIVERSITY IN PRAGUE
FACULTY OF NUCLEAR SCIENCES AND PHYSICAL
ENGINEERING**

Department of Physics



**Strange particle production in jets in pp collisions
in the ALICE experiment**

RESEARCH TASK

**Author: Bc. Vojtěch Pacík
Supervisor: RNDr. Jana Bielčíková, Ph.D.
Consultant: Mgr. Vít Kučera
Academic year: 2014/2015**

Prohlášení

Prohlašuji, že jsem tuto práci vypracoval samostatně a použil jsem pouze podklady uvedené v příloženém seznamu.

Nemám závažný důvod proti užití tohoto školního díla ve smyslu § 60 Zákona č. 121/2000 Sb., o právu autorském, o právech souvisejících s právem autorským a o změně některých zákonů (autorský zákon).

V Praze dne

Title: **Strange particle production in jets in pp collisions in the ALICE experiment**

Author: Bc. Vojtěch Pacík

Field: Experimental Nuclear and Particle Physics (Nuclear Engineering)

Document: Research task

Supervisor: RNDr. Jana Bielčíková, Ph.D.

Nuclear Physics Institute, Czech Academy of Sciences.

Consultant: Mgr. Vít Kučera

Nuclear Physics Institute, Czech Academy of Sciences.

Abstract:

Baryon-to-meson ratio of inclusive strange particles enhancement was observed in heavy-ion collisions at RHIC and the LHC. Study of identified particles in jets can provide a unique way how to investigate this phenomenon and disentangle the effects of extremely hot and dense medium created in such ultra-relativistic collisions on various hadronisation processes and particle production mechanisms. Description of analysis of the K_S^0 and $\Lambda/\bar{\Lambda}$ production in charged jets in proton-proton collisions at centre-of-mass energy $\sqrt{s} = 7$ TeV measured by the ALICE experiment at the LHC is presented.

Keywords: neutral strange particle, baryon anomaly, jets, ALICE, LHC

Název práce: **Produkce podivných částic v jetech v pp srážkách v experimentu ALICE**

Autor: Bc. Vojtěch Pacík

Obor: Jaderné inženýrství

Druh práce: Výzkumný úkol

Vedoucí práce: RNDr. Jana Bielčíková, Ph.D.

Ústav jaderné fyziky, Akademie věd České republiky, v.v.i.

Konzultant: Mgr. Vít Kučera

Ústav jaderné fyziky, Akademie věd České republiky, v.v.i.

Abstrakt:

Při srážkách těžkých iontů na urychlovačích RHIC a LHC byl pozorován zvýšený poměr baryonů vzhledem k mezonům. Studium identifikovaných částic v jetech může poskytnout jedinečný způsob pro zkoumání tohoto jevu a odlišení vlivu velmi horkého a hustého média vznikajícího při těchto ultra-relativistických srážkách vůči různým procesům hadronizace a mechanismů produkce částic. V tomto článku je popsán postup analýzy produkce K_S^0 a $\Lambda/\bar{\Lambda}$ v nabitých jetech v proton-protonových srážkách o těžiškové energii $\sqrt{s} = 7$ TeV změřené experimentem ALICE na urychlovači LHC.

Klíčová slova: neutrální podivné částice, baryonová anomálie, jety, ALICE, LHC

Contents

1	Introduction	4
2	Jets	6
2.1	Cone algorithms	7
2.2	Sequential recombination algorithms	8
2.2.1	k_T algorithm	9
2.2.2	Anti- k_T algorithm	9
2.2.3	Cambridge-Aachen algorithm	9
3	ALICE	11
3.1	Inner Tracking System	12
3.2	Time Projection Chamber	12
3.3	Time-of-Flight detector	13
3.4	Electromagnetic Calorimeter	14
4	Analysis of neutral strange particles production	16
4.1	Data sample	16
4.2	Event selection	17
4.3	V^0 candidate reconstruction	17
4.4	Jets reconstruction	20
4.4.1	V^0 -jet Matching	21
4.5	Signal extraction	25
4.6	Results	29
4.6.1	Inclusive V^0 particles	29
4.6.2	Identified V^0 particles in charged jets	30
5	Summary	38

List of Figures

1.1	Ratio of inclusive neutral strange hadrons	5
2.1	Infrared sensitivity	7
2.2	Collinear sensitivity	7
2.3	Jet shape comparison	10
3.1	A schematic illustration of the ALICE detector	11
3.2	Schema of Inner Tracking System	12
3.3	Scheme of Time-Projection Chamber	13
3.4	Scheme of Time-of-Flight detector	14
3.5	Schema of electromagnetic calorimeters	14
4.1	V^0 topology	18
4.2	p_T -differential spectra of inclusive K_S^0 , Λ and $\bar{\Lambda}$ candidates	19
4.3	η distribution of inclusive K_S^0 , Λ and $\bar{\Lambda}$ candidates	19
4.4	Pseudorapidity distribution of inclusive jets	22
4.5	Azimuthal distribution of inclusive jets	23
4.6	p_T -differential spectra of inclusive jets	24
4.7	V^0 -jet D distribution	25
4.8	Correlation of V^0 p_T and jet leading track p_T	26
4.9	Correlation of (anti-)proton p_T and jet leading track p_T	27
4.10	Correlation of pion p_T and jet leading track p_T	28
4.11	Example of signal extraction method	29
4.12	p_T -differential spectra of inclusive K_S^0 , Λ and $\bar{\Lambda}$	31
4.13	Ratio of inclusive Λ to $\bar{\Lambda}$	31
4.14	Ratio of inclusive neutral strange hadrons	32
4.15	Ratio of inclusive Λ and $\bar{\Lambda}$ to K_S^0	32
4.16	p_T -differential spectra of K_S^0 in jets	33
4.17	p_T -differential spectra of Λ in jets	34
4.18	p_T -differential spectra of $\bar{\Lambda}$ in jets	35
4.19	Ratio of Λ to $\bar{\Lambda}$ in jets	36
4.20	Ratio of Λ and $\bar{\Lambda}$ to K_S^0 in jets	37

Chapter 1

Introduction

In heavy-ion collisions at the ultra-relativistic energies, such as ones achieved at the Large Hadron Collider (LHC) at CERN or Relativistic Heavy Ion Collider (RHIC) at Brookhaven National Laboratory, a new state of nuclear matter of deconfined quarks and gluons is expected to be formed. This state of matter called a quark-gluon plasma (QGP) exists only under extreme conditions such as high temperature and/or density for a very short time. As the conditions change due to the evolution of the bulk a phase transition occurs from these quasi-free partons to the observed final state hadrons (where the partons are confined again).

Hadron identification and its transverse momentum (p_T) spectra and ratios provide a unique tool to study this new state of matter [1]. It was first observed at RHIC at Brookhaven National Laboratory [2,3], that the baryon-to-meson ratio is enhanced in central heavy-ion collisions in comparison with the peripheral or proton-proton (pp) collisions. This enhancement has been observed not only in light flavour hadrons, but also in case of the inclusive strange particles, Λ and K_S^0 (see Figure 1.1). Similar analysis has been done by experiments at the Super Proton Synchrotron (SPS) and later at the LHC [4] at CERN both in pp and heavy-ion collisions.

This so-called “baryon anomaly” phenomenon is still not fully understood, although various models are currently under investigation, namely parton fragmentation and hadronisation modification, parton recombination [5] and radial flow [6].

Parton fragmentation and following hadronisation is a well-known mechanism of perturbative theory of Quantum Chromodynamics (QCD). In hard scattering processes occurring in early stages of a collision, high- p_T parton may be created. This hard parton then fragments and subsequently hadronises into a number of collimated softer particles (softer in a sense of smaller p_T). However fragmentation in the QCD vacuum alone cannot explain this anomaly. On the other hand, in strongly interacting medium, such as QGP, parton fragmentation may be modified due to the interactions with its constituents, i.e. deconfined quarks and gluons.

Parton recombination is a phenomenon, which assumes that three quarks or quark/anti-quark pair in the densely populated phase-space may cluster together and therefore create a baryon or meson respectively [5]. To form a hadron, much less energy is needed for the quarks in parton recombination model than for the fragmentation mechanism. This process is possible up to few GeV/ c , then its probability quickly drops.

Collective effects such as radial flow may also influence the baryon-to-meson ratio, due to the fact that heavier particles are pushed towards higher p_T , which supports by the

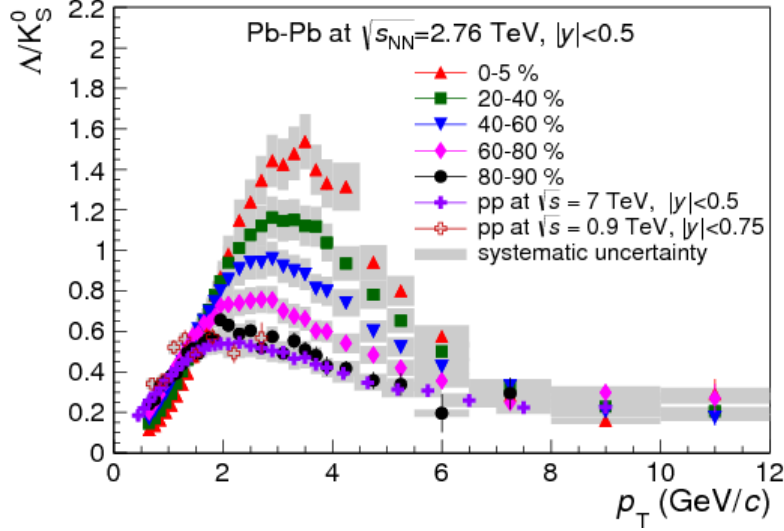


Figure 1.1: Ratio of inclusive production of neutral strange Λ baryons and K_S^0 mesons [4] illustrating the so-called baryon anomaly, the enhancement of baryon production with respect to the meson production in Pb-Pb relative to the pp collisions.

similar arguments possible baryon enhancement in the region of higher momentum. A study of radial flow ordering with respect to the strange content of the particles may bring additional insights to the matter [7].

The main motivation of study of neutral strange particles production in jets is to understand the origin of discussed baryon anomaly (enhancement of $\Lambda/\bar{\Lambda}$ baryons with respect to the K_S^0 mesons) and distinguish between the possible effects of hot and dense strongly interacting medium and other discussed mechanism (in general distinguish so-called soft and hard processes) by comparing identified hadrons in jets with inclusive hadrons produced by the thermalized bulk. Additional aspect of such analysis in pp collisions is providing a suitable reference for currently undergoing studies both in Pb-Pb and p-Pb collisions.

In the following Chapter 2 I will introduce the basic concept of jets and briefly discuss the methodology of various jet reconstruction algorithms. In Chapter 3, the ALICE (A Large Ion Collider Experiment) detector will be described including the detecting subsystems involved in the analysis of neutral strange K_S^0 and Λ particles in charged jets in pp collisions at $\sqrt{s} = 7$ TeV, which will be reported in detail in Chapter 4.

Chapter 2

Jets

According to the perturbative theory of Quantum Chromodynamics (QCD), a highly virtual parton, quark or gluon, can be generated in a hard scattering occurring during very first moments of high-energy collisions such as those at the largest particle colliders. These partons are not directly observable, instead one can observe jets, collimated showers of particles resulting from fragmentation and hadronisation of the initially very energetic or hard¹ partons.

Proper reconstruction and following physical interpretation of jets is therefore crucial for correct understanding of QCD aspects according to the current knowledge. From an experimental point of view searching for bunches of collimated final state hadrons may seem like a rather trivial task, especially in case of proton-proton collisions, where multiplicities are relatively low with regards to collisions of heavy-ions. But for accurate comparison of predictions at parton level and experimentally observable particles well-defined jet-finding procedure is essential.

The jet-finding procedure begins with a list of “particles”. These can be partons on the level of theoretical simulation or hadrons registered as a signal on the detector level (e.g. particle tracks or energy deposited in calorimeters). Particles that are close to each other in terms of azimuthal and polar angles are generally called clusters. Purpose of jet finding algorithm (jet-finder) is to select and associate particles and clusters into more complex objects - jets - according to certain well-defined rules. This part of jet-finder is called “jet algorithm”. The kinematic properties of the particles such as energy or four-momentum have to be assigned to a jet as well. This is called a “recombination scheme”. The difference between various jet-finders is therefore given by using a specific jet algorithm and/or recombination scheme.

For an ideal jet-finder following features are expected. The first one is infrared safety. Final jets resulting from the jet reconstruction procedure should be insensitive to any soft radiation, meaning that addition or subtraction of a single hadron with low p_T should not change the properties of final reconstructed jet, such as shape or direction of its axis, as can be seen in Figure 2.1.

The second one is collinear safety illustrated in Figure 2.2. Imagine a single parton shower that is at the detector level registered as two independent signals separated by the almost zero distance, for instance in two neighbouring calorimeter cells. Such signals may in general change the resulting jet or not be identified as a jet at all (e.g. they may not pass the energy threshold needed for distinguishing detector noise from the signal).

¹Hard in a sense of high transverse momentum p_T . On the other hand, particles or partons with relatively low p_T is considered as soft.

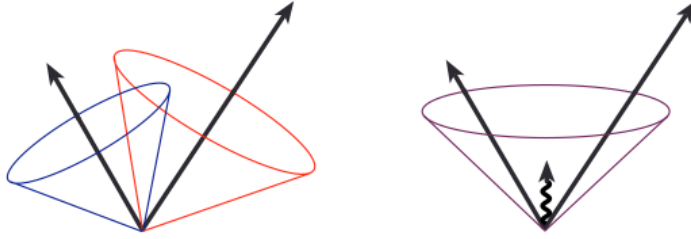


Figure 2.1: Illustration of infrared sensitivity. On the left hand side, two reconstructed jets can be seen. Adding soft radiation (in this example, low- p_T gluon) may change the outcome of the recombination procedure, as can be seen on the right hand side, where only one jet is reconstructed instead of original two jets [8].

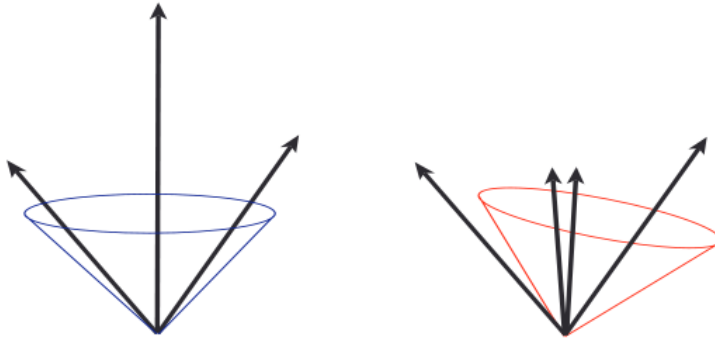


Figure 2.2: Illustration of collinear sensitivity. Registered signal (such as the middle one on the left hand side) may be registered as two independent signals due to the technical specifications of the detector, e.g. in two neighbouring cells, as can be seen on the right hand side. This can therefore clearly affect the properties of the resulting jet [8].

In addition, the ideal jet algorithm should be invariant under Lorentz boost in longitudinal direction, its reconstruction solution should be the same at parton, particle and detector level and also should be experiment and detector independent. Last but not least, considering the large amount of data expected to be processed, it should be as efficient as possible from point of view of computing time.

In general, one can distinguish two types of jet-finding algorithms, cone and sequential recombination algorithms [8].

2.1 Cone algorithms

The basic idea of a jet cone algorithm is to associate the particles in a circular area with a specific radius R in $\phi \times \eta$ space, where ϕ is an azimuthal angle and η is pseudorapidity given by $\eta = -\ln \tan \frac{\theta}{2}$, where θ is a polar angle.

For each circle, its energy weighted centroid is estimated (i.e. according to the energy distribution of the particles within the area), which becomes a new geometric centre of the circle. With respect to the particles in this new area, a new centroid is estimated. This process continues until a stable cone is found, meaning that the geometric centre of the circular area is aligned with the centroid of energy deposition in the centre.

This rather simple jet finding algorithm could scan the whole detector and find all stable cones by simply using each space point as the initial centre. However, this may turn out to be a quite time consuming process due to the large granularity of the current detectors and high number of particles. Therefore, the need for selecting more physically important starting points had arisen and the idea of so-called seeds was introduced [8] in order to reduce the required CPU time.

In case of cone algorithms with seeds, $\phi \times \eta$ space is scanned and all particles with energy larger than specified threshold are tagged as seeds. These seed are then used as initial geometric centres, starting points of the jet algorithm. Although the seed algorithm is much faster than the seedless one, there is also a problem with such algorithm. The cone algorithm with seed is not collinear safe and is also quite sensitive to soft radiation. Situation may be improved by adding so-called midpoints in between the seeds².

The remaining issue with both algorithms with seeds and seedless ones that should be noted is the fact, that particles may be associated with more than one jet reconstructed with the cone algorithm. Overlapping cones need to be merged or split in order to solve this physical problem. Basic condition to decide whether two overlapping cones should be merged or not is based on a shared energy fraction f relative to the one with less energy. If the less energetic cone shares more than f of its energy, two cones are merged, otherwise they are split according to the distance of shared particles.

The SIScone algorithm is the most commonly used cone algorithm. This seedless cone algorithm is not only infrared but also collinear safe in all orders of the perturbation theory [9]. SIScone searches for all possible stable cones, even though it is a relatively fast algorithm (with the complexity of $N^2 \log N$), for large number of initial particles is rather impractical.

2.2 Sequential recombination algorithms

The sequential recombination algorithms have been developed in contrast to the cone algorithms. These algorithms successively merge a pair of particles in order of the increasing relative transverse momentum p_T .

First, the list of all particles (also known as preclusters) is created and four-momentum (E_i, \vec{p}_i) is assigned to each of them. For each pair of particles $(i, j), i \neq j$, parameter d_{ij} is defined in following way

$$d_{ij} = \min(p_{T,i}^{2p}, p_{T,j}^{2p}) \frac{\Delta R^2}{R^2}, \quad (2.1)$$

where ΔR (2.2) is distance between particles in $\eta \times \phi$ space. The R is a jet resolution parameter, which is similar to the cone radius and reflects the approximate shape of the jet. Contrary to the rather circular cones, jets reconstructed via sequential recombination algorithms do not exhibit fixed conical shape (See Figure 2.3). The power of p_T $p = 1$ for

²In practice, midpoints may be placed in the positions $p_i + p_j$ or $p_i + p_j + p_k$, where p_i, p_j, p_k are seeds four-momenta.

k_T , $r = -1$ for anti- k_T and $r = 0$ for Cambridge-Aachen algorithm.

$$\Delta R = \sqrt{(\eta_i - \eta_j)^2 + (\phi_i - \phi_j)^2} \quad (2.2)$$

For each particle parameter d_i given by $d_i = p_{T,i}^2$ is estimated. Then the minimum d_{min} is found among d_{ij} and d_i of all particles.

If the $d_{min} = d_{ij}$, the particles i and j are merged, removed from the list of all particles and replaced with new particle coming from merging i, j according to the given recombination scheme. Otherwise, if $d_{min} = d_i$ then the particle i cannot longer be merged and is therefore removed from the list and identified as jet. Then the new values of d_i and d_{ij} are calculated. This process is repeated until the list of particles is empty. Also, since the particle assigned to the particular jet is removed from the list and therefore no longer available, the complicated situation similar to the overlapping cones is not possible.

Various algorithms may differ in condition of termination. The alternative to the one mentioned above is comparing d_{min} with a specific d_{cut} . When the $d_{cut} > d_{min}$ the merging procedure is finished. Additionally, for the proper application of sequential jet finding algorithm, the choice of the recombination scheme is required.

2.2.1 k_T algorithm

As can be seen from (2.1), k_T algorithm merges the closest particles with smaller p_T first, which reflects the QCD splitting [10]. Probably the most important note to mention is the fact, that k_T algorithms are by design infrared and collinear safe.

On the other hand, since k_T algorithms work with almost every particles during clustering process they are quite demanding regarding the CPU time, but they are still faster than seedless cone algorithms. The algorithmic complexity of the first k_T algorithms was scaled as N^3 , where N is total number of initial preclusters. This fact would have been an critical obstacle to typical multiplicities achieved in collisions at LHC energies. Luckily, the implementation of **FastJet** k_T jet-finder algorithm [11] improves the complexity to the scale of $N \ln N$, which makes it the fastest jet-finder available for $N \geq 10^4$ [12].

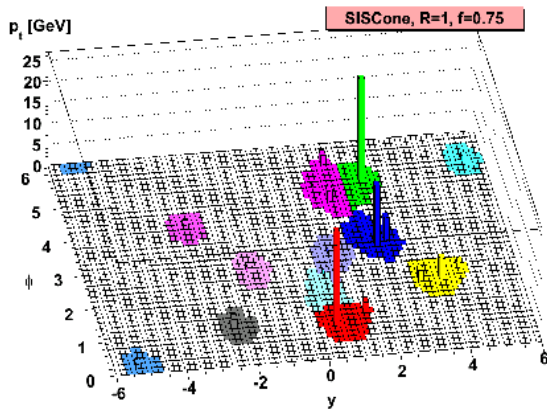
2.2.2 Anti- k_T algorithm

For the k_T algorithm the particles are merged in order of ascending p_T . But as it eventually turned out, more suitable choice is $p = -1$. The latter is known as the anti- k_T algorithm [13], which clusters the particles from the hardest to the softer ones.

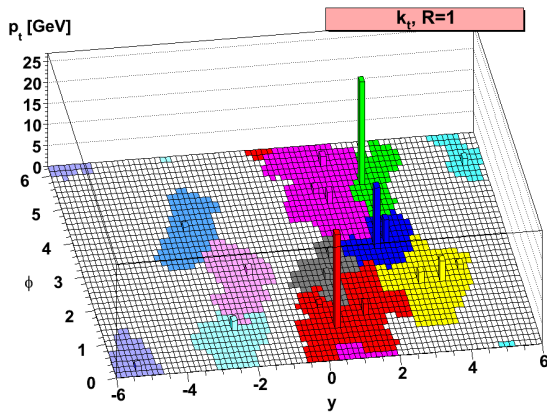
This method naively reflects the idea of fragmentation, where initially hard parton radiates the ones with smaller p_T . This may be interpreted as going reverse in time from final state hadrons registered in detector to the initial partons created during early phase of the collision.

2.2.3 Cambridge-Aachen algorithm

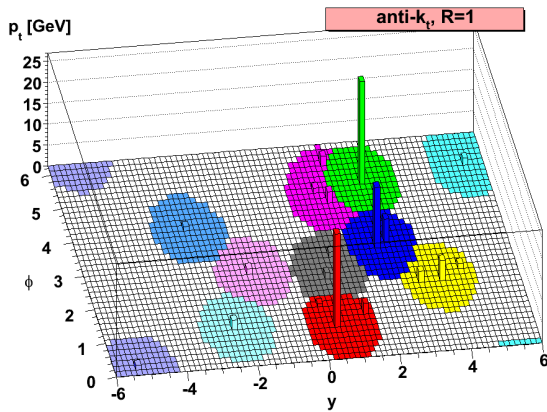
Since the d_{ij} parameter is no longer dependent on p_T , the Cambridge-Aachen jet finding algorithm reconstructs jets only on the basis of preclusters angular distribution. It clusters the pairs with smallest angle first, but also provides a lower limit, when the clustering of small-angle jet pair is no longer possible, if one of the jets is too soft [14].



(a) SIScone



(b) k_T



(c) anti- k_T

Figure 2.3: Jet shape comparison of various reconstruction algorithms [13]. In all three cases the simulated event is the same, only the jets are result of using various jet reconstruction algorithms with same jet resolution parameter $R = 1$, namely: (a) SIScone cone algorithm, (b) k_T clustering algorithm and (c) anti- k_T clustering algorithm.

Chapter 3

ALICE

ALICE (A Large Ion Collider Experiment) is one of the four large experiments and the only experiment dedicated to study of ultra-relativistic heavy-ion collisions situated at the LHC at CERN. ALICE is therefore optimized for extremely high multiplicities and designed to be complementary to the other experiments situated at the LHC, namely ATLAS, CMS and LHCb.

ALICE is a multipurpose detector consisting of a total number of 18 various detecting sub-systems situated in one of the two main sectors: central barrel detectors or forward muon spectrometers.

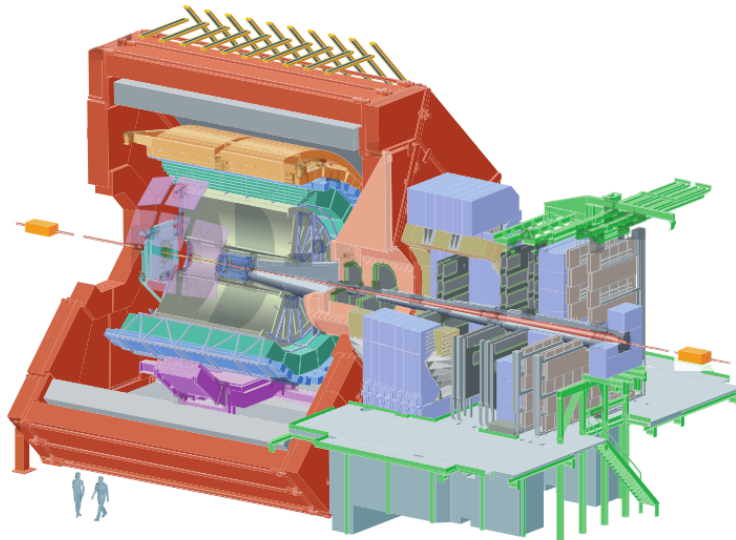


Figure 3.1: Schematic illustration of ALICE detector [15].

Forward muon spectrometers, as the name suggests, contain detectors for measuring μ^+ , μ^- primarily coming from leptonic decays of ϕ meson or heavy-flavour quarkonia (bound states of $q\bar{q}$ pairs of the same flavour), such as J/ψ and Υ .

Central barrel detectors, covering polar angle region from 45° to 135° (corresponding to approximate pseudorapidity coverage of $|\eta| \leq 0.9$) and full azimuth, are embedded in a large solenoidal magnet with nominal magnetic field of 0.5 T from the superseded L3 experiment at LEP (Large Electron Positron collider). Main purpose of this detector system is tracking and particle identification (PID) of hadrons, electrons and photons.

In following sections, only detection systems that are particularly relevant to the discussed analysis of neutral strange particles production in jets or to jet analysis in general are described. A more detailed description of the whole ALICE detector and its sub-systems can be found in [15].

3.1 Inner Tracking System

The main tasks of the Inner Tracking System (ITS) are the localization of a primary vertex (PV) or an interaction point, the point along the beam direction z -axis, where the collision occurs and reconstruction of secondary vertices of heavy-flavour hadrons, such as D and B mesons, and hyperons decays (particles containing at least one strange quark, e.g. Λ). The ITS is also capable of tracking and PID of hadrons with p_T from 200 MeV/ c and therefore improves the tracking resolution and overall possibilities of main tracking detector of ALICE experiment, the Time-Projection Chamber.

The ITS consists of three pairs of cylindrical layers of silicon detectors surrounding the beryllium beampipe and thus it is the closest detector with respect to the primary vertex with transverse distance ranging from 4 to 43 cm. First two layers are Silicon Pixel Detectors (SPD) chosen to fulfill the requirements for high precision of PV identification and high particle density. Then follows the two layers of Silicon Drift Detectors (SDD) and two outer layers are made of Silicon Strip Detectors (SSD).

Contrary to the SPD, these four outer layers are equipped with an analogue readout chip, allowing to estimate the characteristic dE/dx ionization losses of non-relativistic low momentum particles together with really low material budget of 5% of radiation length X_0 .

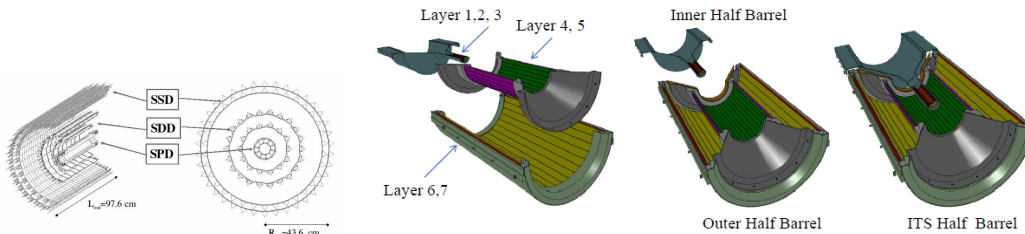


Figure 3.2: Schematic illustration and radial cross-section of ITS consisting of three pairs of silicon pixel detectors.

3.2 Time Projection Chamber

The specifications of the Time Projection Chamber (TPC) provide the unique capabilities both for tracking and particle identification. It is used as a main tracking detector in central barrel providing up to 159 space-points per track with good two-track separation and momentum resolution in wide range of p_T from 0.1 GeV/ c up to 100 GeV/ c . The TPC is capable of proton, kaon, pion and electron identification up to order of tens GeV/ c with good particle identification separation.

By design, the TPC is a cylindrical drift detector with multi-wire proportional chambers on each side and overall pseudorapidity coverage of $|\eta| \leq 0.9$ consisting of field cage with

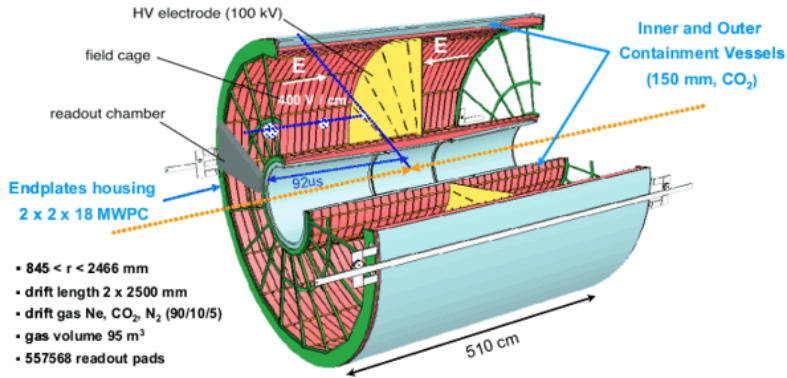


Figure 3.3: Schema and technical specifications of the ALICE Time-Projection Chamber.

dimensions of 500 cm in beam direction and inner and outer radii of 85 and 247 cm, respectively, filled with approximately 90 m³ of Ne/CO₂/N₂ mixture.

The TPC was designed to fully withstand the huge particle densities, which were first estimated by extrapolating the RHIC data to the LHC energies [15]. Based on this data, it means more than 20 000 charged particles (both primary and secondary) inside the TPC. In case of Pb-Pb collisions, the TPC was designed to operate with a frequency of 200 Hz, making the TPC the “slowest” sub-system of ALICE. This disadvantage is one of the important tasks discussed for future upgrades of the ALICE detector.

3.3 Time-of-Flight detector

In addition to the TPC, the Time-of-Flight (TOF) detector is used for particle identification of pions and kaons up to 2.5 GeV/*c*, and protons with maximal *p*_T of 4 GeV/*c*. It also provides good *K*/*π* and *K*/*p* separation.

The TOF detector is a 141 m² cylindrical array of gaseous Multi-gap Resistive Plate Chambers situated at radial distance of 370 cm to the beampipe with coverage $|\eta| \leq 0.9$ in pseudorapidity and full in azimuth except a relatively small area in front of the Photon Spectrometer due to the material reduction.

Time-of-flight particle identification method is based on proper estimation of time interval between the collision and the moment when a particle arrives to the TOF detector (so-called arrival time). Since the distance from the interaction point to the TOF is well-defined, with this information, one can estimate the velocity of the measured particle. Additionally, if the particle momentum is known, the mass can be derived and therefore one can identify the detected particles.

The starting time is estimated via a T0 detector, which is a pair of Cherenkov counters located near the beampipe opposite to each other with centre of the ITS in between them. Besides the time to the TOF detector, it provides information about primary vertex position and is also used as the lowest level L0 trigger.

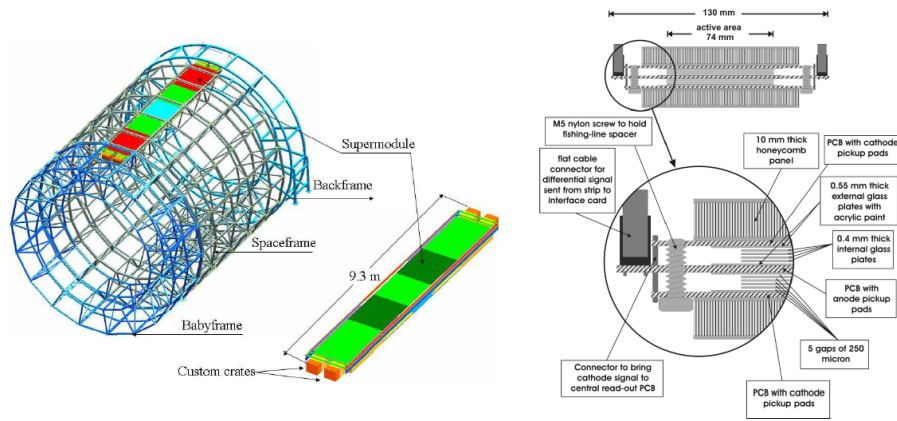


Figure 3.4: Schema of the ALICE TOF detector (left hand side) and specifications of its module (right hand side).

3.4 Electromagnetic Calorimeter

Since most of the detecting systems mentioned in previous sections operate only with charged particles, the need for a detector of electrically neutral particles have arisen, especially in the field of jet studies, where the fragmentation processes may lead to the creation of relatively large number of such neutral and thus undetectable particles. Consequently, one has to choose whether to reconstruct charged jets, where information based only on detector response of charged particles is used; or the full jets including also the information about neutral part of the hadronic content of the jets. The latter was made possible by including an Electromagnetic Calorimeter (EMCal) among the ALICE detectors.

The EMCal is a Pb-scintillator sampling calorimeter located 4.5 m from the beampipe with overall acceptance of $|\eta| \leq 0.7$ in pseudorapidity and 107° in azimuth. This limited coverage with respect to the other detecting sub-systems is due to the lack of free space available inside the L3 coil and the fact that the EMCal was not considered from the very beginning of the ALICE design, but added later in order of address the question of jet quenching phenomena.

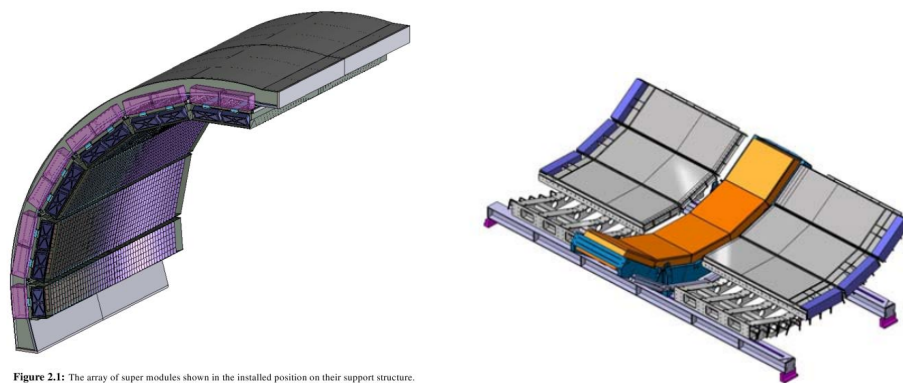


Figure 2.1: The array of super modules shown in the installed position on their support structure.

Figure 3.5: Schematic illustration of the EMCal (left hand side) and its upgrade DCal (right hand side).

Implementation of a new Di-jet Calorimeter (DCal) detector in the area opposite to

the EMCal will significantly improve the current situation with calorimetry in ALICE. The addition of the DCal will allow in LHC Run 2 more precise measurement of jets spectra as well as more detailed study of physically interesting phenomena such as dijets (two jets originating in the same spot but propagating in almost opposite directions).

Chapter 4

Analysis of neutral strange particles production

In this section, concept of the analysis of K_S^0 , Λ and $\bar{\Lambda}$ in charged jets in proton-proton collisions at $\sqrt{s} = 7$ TeV is presented. Analysis is conducted by the ALICE analysis task class `AliAnalysisTaskV0sInJetsEmcal` in the following steps:

1. Event selection
2. Topological selection of inclusive V^0 candidates
3. Inclusive jets reconstruction
4. Selection of V^0 candidates associated with jets
5. Yield estimation via signal extraction¹

4.1 Data sample

For this analysis, real data from proton-proton (pp) collisions at centre-of-mass energy $\sqrt{s} = 7$ TeV taken in LHC Run 1 by the ALICE detector in the year 2010 have been used. Specifically, datasets from pass2 reconstruction cycle of LHC10d and LHC10e periods listed in the good run list `LHC10d_AOD135` and `LHC10e_AOD135` with flat ϕ distribution. Mentioned good run lists are commonly used for studies of charged jets in pp collisions within the Physics Working Group Jets (PWG-JE).

Numbers of used runs included in the `LHC10d_AOD135` are following: 122374, 125023, 125085, 125097, 125100, 125101, 125134, 125139, 125140, 125156, 125186, 125296, 125630, 125632, 125633, 125842, 125843, 125844, 125847, 125848, 125849, 125850, 125851, 125855, 126004, 126007, 126008, 126073, 126078, 126081, 126082, 126088, 126090, 126097, 126158, 126284, 126285, 126351, 126352, 126359, 126403, 126404, 126405, 126406, 126407, 126408, 126409, 126422, 126424, 126425, 126432, 126437.

And in the `LHC10e_AOD135`: 127712, 127714, 127718, 127719, 128495, 128498, 128503, 128504, 128505, 128507, 128605, 128615, 128621, 128677, 128678, 128777, 128778, 128820, 128823, 128824, 128833, 128835, 128836, 128843, 128850, 128853, 128855, 128913, 129512, 129513, 129514, 129599, 129639, 129641, 129652, 129653, 129654, 129659, 129667, 129960,

¹Not included in analysis task class `AliAnalysisTaskV0sInJetsEmcal`.

129961, 130157, 130158, 130179, 130519, 130601, 130608, 130696, 130704, 130793, 130798, 130799, 130834, 130840.

Total number of events before applying the selection criteria included in the runs listed above is more than 185 million.

4.2 Event selection

Only minimum bias (MB) events with selection tag `AliveEvent::kMB` and following additional conditions concerning primary vertex (PV) have been used:

- number of contributors greater than 2,
- z distance between PV and interaction point smaller than 10 cm,
- radial distance r from beam axis smaller than 1 cm,
- reconstructed from SPD and TPC, but not based only on TPC,
- distance between nominal PV and SPD-only reconstructed PV smaller than 0.1 cm.

After applying selection criteria data sample used in this analysis contained approximately 135 million events.

4.3 V^0 candidate reconstruction

Neutral strange particles decay via the weak interaction into a pair of daughter particles with opposite charge (see Table 4.1). In presence of homogenous external magnetic field these two particles travel in such directions that the characteristic “V-shaped” decay geometry can be observed. K_S^0 and $\Lambda/\bar{\Lambda}$ particles are therefore referred to as V^0 for their characteristic decay topology, which can be described by the following parameters (see Figure 4.1).

Decay channel	Branching Ratio [%]	Mother mass [MeV/ c^2]	Mean lifetime [ps]
$K_S^0 \rightarrow \pi^+ + \pi^-$	69.2	497.61	89.56
$\Lambda \rightarrow p + \pi^-$	63.9	1115.68	263
$\bar{\Lambda} \rightarrow \bar{p} + \pi^+$	63.9	1115.68	263

Table 4.1: V^0 decay channels [16].

- **Daughter tracks Distance of Closest Approach (DCA)** Minimal distance between the two daughter tracks
- **Primary vertex (PV)** Point, where the collision occurs
- **Secondary vertex (SV)** Point in the middle of the daughter tracks in their DCA
- **DCA to the PV** Minimal distance between the daughter tracks and the primary vertex
- **Decay radial length** Distance between the primary vertex and the secondary vertex
- **Cosine of pointing angle (CPA)** Cosine of the angle between the PV and the SV line and V^0 momentum

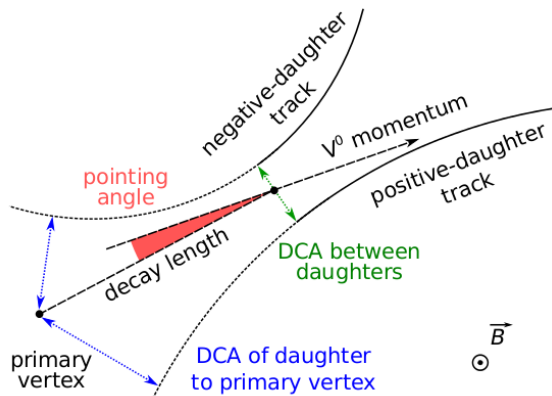


Figure 4.1: Characteristic topology of neutral strange particles decays [17].

V^0 candidate selection was conducted by an offline method based on the various topological criteria and kinematical cuts in order to suppress as much combinatorial background as possible without losing too many signal particles. Values of these cuts were chosen to be in agreement with the analysis of inclusive K_S^0 and $\Lambda/\bar{\Lambda}$ production in pp collisions performed in the Physics Working Group Light Flavour (PWG-LF) [18]. The complete list of cuts and selection criteria is presented in Table 4.2.

Parameter	Value
Reconstruction method	offline
Track TPC refit	<code>AliAODTrack::kTPCrefit</code>
Vertex tracks type	<code>!AliAODVertex::kKink</code>
Number of findable TPC clusters	> 0
Number of crossed TPC rows	≥ 70
Crossed TPC rows over findable clusters	≥ 0.8
Daughter DCA to PV	≥ 0.6 mm
DCA between daughters	$\leq 1\sigma$ (TPC tracking)
CPA (K_S^0)	≥ 0.97
CPA ($\Lambda/\bar{\Lambda}$)	≥ 0.995
Decay radial length r	$5 \leq r \leq 100$ cm
Track pseudorapidity	$ \eta \leq 0.8$
V^0 pseudorapidity	$ \eta \leq 0.7$
V^0 candidate mass	$< 3\sigma$ (PDG)
Proper life-time (K_S^0)	$\leq 7.45 c\tau$
Proper life-time ($\Lambda/\bar{\Lambda}$)	$\leq 3.8 c\tau$
Armenteros-Podonaski cut (K_S^0)	$p_T^{\text{Arm}} \geq 0.2 \alpha $

Table 4.2: Selection cuts and criteria for daughter tracks and inclusive V^0 candidates.

First, the standard quality cuts for charged V^0 candidate's daughter tracks were applied, such as a minimum value of number of crossed TPC rows over number of findable TPC clusters ratio and a pseudorapidity acceptance cut. In addition, TPC refit was done and kink tracks were rejected. Kink tracks are tracks that cannot be properly reconstructed because of the insufficient efficiency of tracking, instead they have been split and subsequently merged during the reconstruction process.

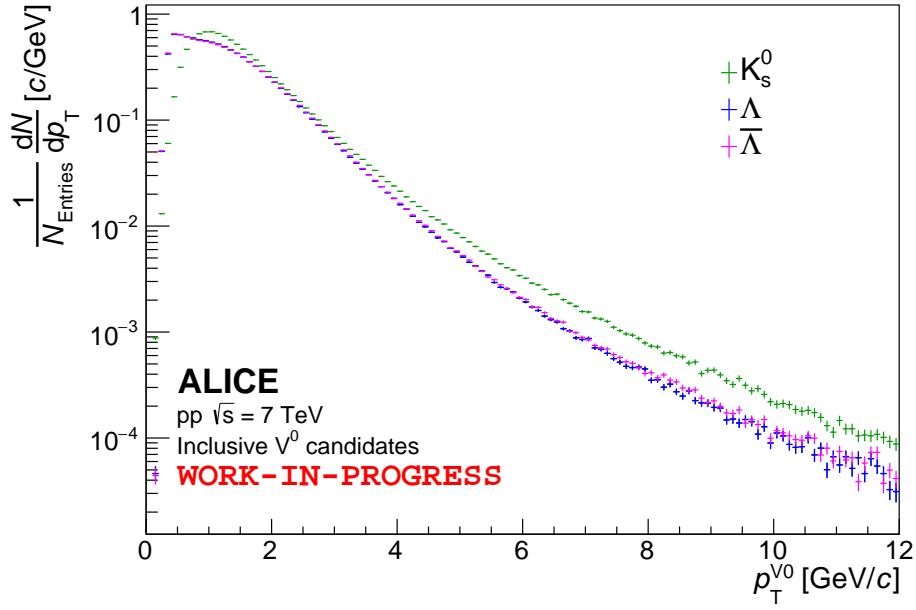


Figure 4.2: An uncorrected p_T -differential spectra of inclusive K_S^0 , Λ and $\bar{\Lambda}$ candidates before conducting the signal extraction method.

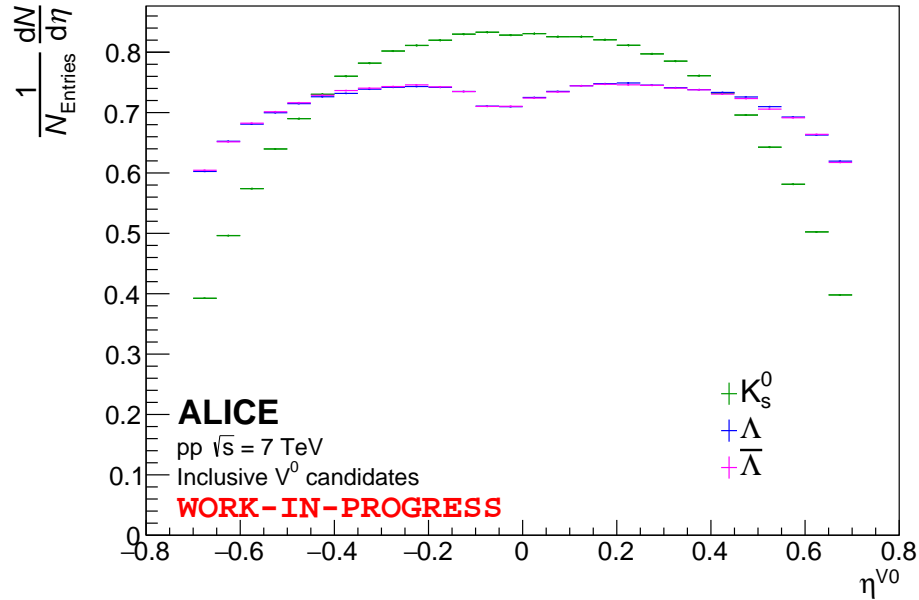


Figure 4.3: An uncorrected η distribution of inclusive K_S^0 , Λ and $\bar{\Lambda}$ candidates normalized by the number of entries before conducting the signal extraction method.

Then the topological cuts listed above were applied. In this analysis particle identification (PID) of V^0 daughters via the TPC dE/dx information was not applied, since it has no significant effect for particles with p_T greater than 2 GeV/ c [17].

Finally, the pseudorapidity cut of reconstructed V^0 candidates and the particle dependent criteria was applied for a proper life-time in transverse plane² and the Armenteros-Podolanski α variable³.

From the initial number of more than 180 million events, 74 million events with at least one V^0 candidate was selected after applying all the criteria and cuts mentioned in this and previous sections. An uncorrected p_T -differential spectra and η distributions of inclusive K_S^0 , Λ and $\bar{\Lambda}$ candidates passing selection criteria are shown on Figure 4.2 and Figure 4.3, respectively. Since the V^0 reconstruction efficiency or feed-down subtraction (Ξ decaying into $\Lambda/\bar{\Lambda}$) is not included, note that all of the distributions and spectra will be referred to as uncorrected or raw from now on.

4.4 Jets reconstruction

For estimation of strange particles yield in jets, jet reconstruction is needed to be done in parallel with V^0 reconstruction. Inclusive jets are therefore independent of V^0 reconstruction procedure.

In this particular analysis, only the charged jets were reconstructed, meaning that trajectories of charged particles passing selection criteria listed below were clustered with no additional information from electromagnetic calorimeters about electrically neutral part of the parton shower. In addition the tracks used for jet reconstruction had to fulfill certain detection quality criteria, commonly used within the PWG-JE, referred to as “hybrid tracks” [19].

- Tagged as a “hybrid track”
- Minimum track p_T of 150 MeV/ c
- Pseudorapidity range in detector acceptance $|\eta^{\text{track}}| < 0.9$

Tracks passing listed requirements served as an input for jet reconstruction algorithm carried by sequential recombination anti- k_T algorithm from the **FastJet** package [20] and implemented in AliPhysics class **AliEmcalJetTask** with following parameters.

- Jet resolution parameter $R = 0.2, 0.3, 0.4$
- Charged jets
- p_T recombination scheme

After the jet-finding procedure additional selection criteria listed below was applied in order to suppress the combinatorial jets and increase the probability of selecting the hard-scattering processes. For proper interpretation of comparison between inclusive V^0 production and production of identified V^0 associated with jet, the additional condition of a whole jet cone lying inside V^0 acceptance was introduced.

²Estimated as $c\tau = \frac{rmc^2}{p_T c}$, where r is the decay radius in $x \times y$ plane.

³Given by $\alpha = \frac{q_L^+ - q_L^-}{q_L^+ + q_L^-}$, where q_L^i is a daughter longitudinal momentum with respect to the mother total momentum.

- Minimum jet p_T of 5 GeV/ c , 8 GeV/ c , 10 GeV/ c , 12 GeV/ c
- Minimum jet leading charged track⁴ p_T of 0 GeV/ c , 3 GeV/ c
- Minimum jet area $A = 0.6\pi R^2$
- Full jet inside pseudorapidity acceptance of V^0 $|\eta^{\text{jet}}| < |\eta^{V^0}| - D$

The parameter D has a similar meaning as the jet resolution parameter R and it was used for the purpose of V^0 -jet matching procedure.

An uncorrected η and ϕ distributions and p_T -differential spectra of reconstructed charged jets fulfilling the requirements mentioned in this section are shown on Figure 4.4, Figure 4.5 and Figure 4.6 respectively for different values of minimum jet p_T and minimum jet leading track p_T cuts in combination with three different values of jet resolution parameter R .

4.4.1 V^0 -jet Matching

V^0 matching procedure have been done on the geometrical basis. The only criterion for associating the V^0 candidate with the jet is following. If the distance in $\eta \times \phi$ space between the V^0 candidate p_T and jet axis $\Delta R = \sqrt{(\eta^{\text{jet}} - \eta^{V^0})^2 + (\phi^{\text{jet}} - \phi^{V^0})^2} \leq D$ is smaller than certain value represented by the jet-matching parameter D , then the V^0 is considered as associated with the jet (“InJet” V^0). In this analysis, the value of D parameter was set equal to the value of jet resolution parameter R .

The distribution of distance D between inclusive V^0 candidate and the closest jet axis is presented on Figure 4.7 together with the jet fraction (ratio of number of jet associated with V^0 candidates and total number of inclusive reconstructed jets) for various values of D (in the same sense as R used in this analysis). It represents the approximate fraction of selected V^0 candidate associated with jets relative to the all reconstructed jets depending on the D cut (or the R , since they are same) value used.

Figure 4.8 shows the correlation between the p_T of the selected V^0 candidates associated with jet and its leading track p_T for Λ and $\bar{\Lambda}$ particles. It indicates that in the region of intermediate p_T up to 8 GeV/ c the most of the V^0 momentum is carried out by the leading hadron inside the associated jet. Additionally, Figure 4.9 indicates that the leading hadron in the associated jet is (anti-)proton from Λ ($\bar{\Lambda}$) decays.

Contrary to the $\Lambda/\bar{\Lambda}$ case, K_S^0 candidates associated with jets shows no such significant correlation between daughter p_T and the leading track p_T in associated in the particular jet (as can be seen on Figure 4.10).

Note that in all Figures mentioned above the candidate cross-contamination is present, since the V^0 s are only the candidates before the signal extraction procedure is conducted, not the selected V^0 s.

Figures 4.8, 4.9 and 4.10 also represent the sensitivity of the yields of identified V^0 associated with jets to the jet leading track p_T cut. Since most of the K_S^0 candidates are associated with jets with low leading hadron p_T , applying a high leading track p_T selection criterion may introduced a bias to the sample. This may play an important role in Pb-Pb and p-Pb analyses, where the leading track p_T cut is used for suppressing soft combinatorial jets.

⁴Leading track means the hardest track or track with highest p_T inside the jet cone.

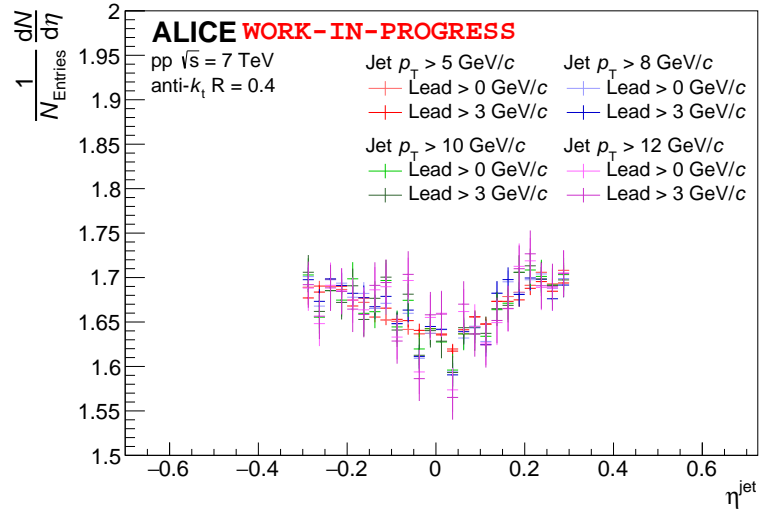
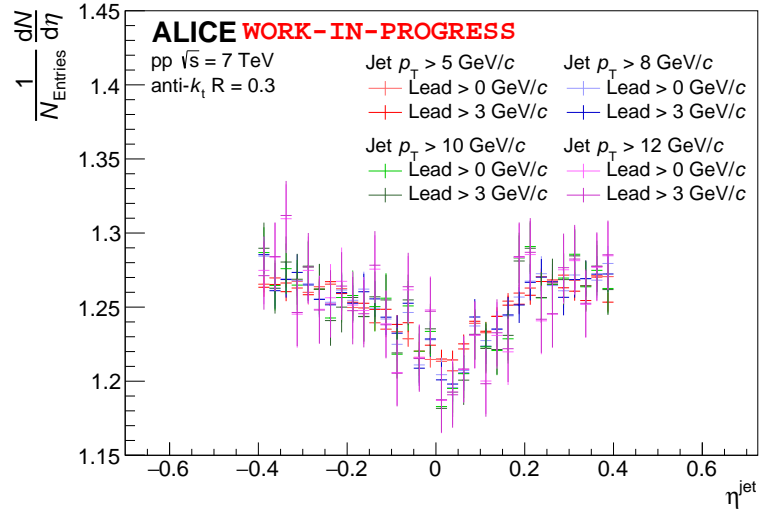
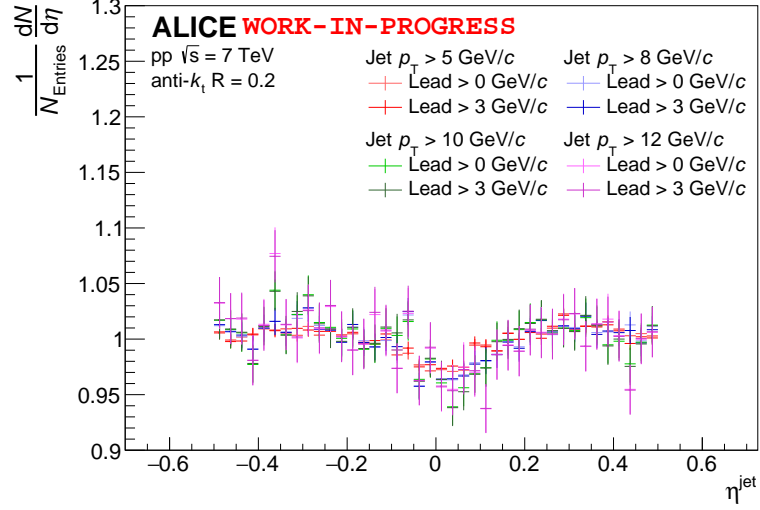


Figure 4.4: Pseudorapidity (η) distribution of reconstructed inclusive charged jets in pp collisions at $\sqrt{s} = 7$ TeV/c for the three values of the jet resolution parameter $R = 0.2$ (top), 0.3 (middle), 0.4 (bottom) and various combinations of minimum jet p_T and minimum jet leading track p_T cut normalized by the number of events (see legend). Please note the zero-suppressed y -axis scale.

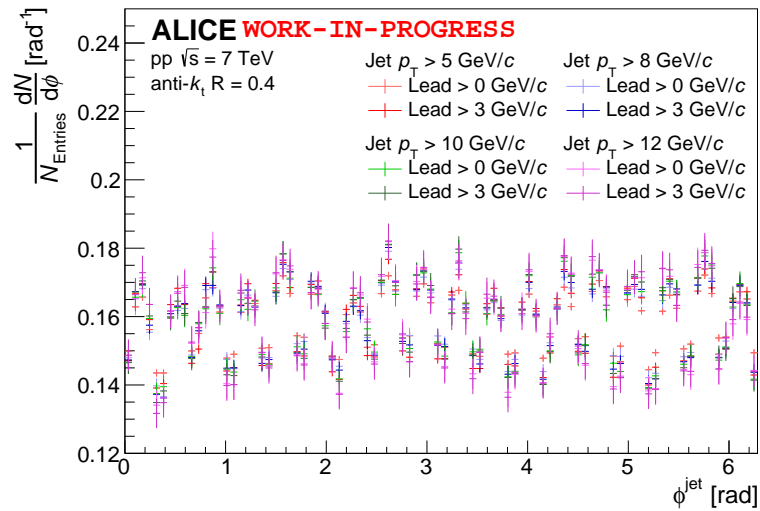
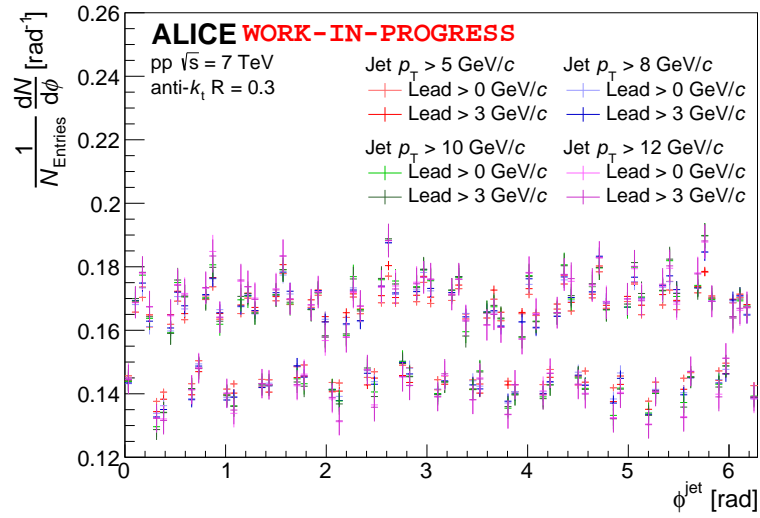
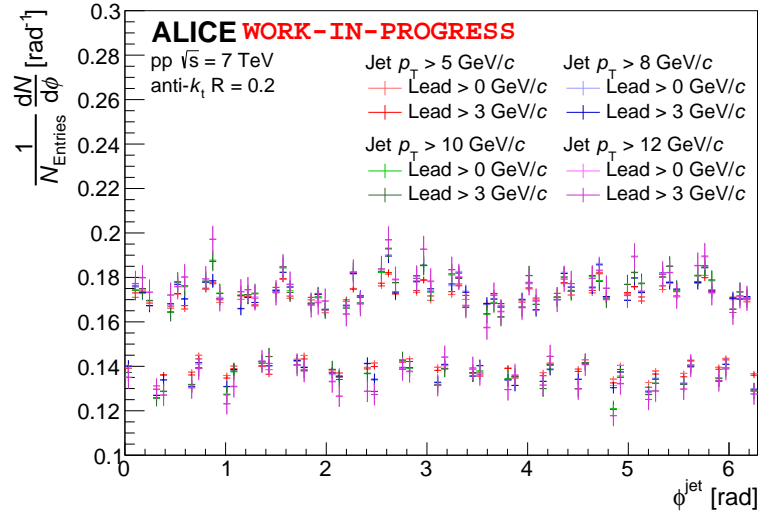


Figure 4.5: Azimuthal (ϕ) distribution of reconstructed inclusive charged jets in pp collisions at $\sqrt{s} = 7$ TeV/c for the three values of the jet resolution parameter $R = 0.2$ (top), 0.3 (middle), 0.4 (bottom) and various combinations of minimum jet p_T and minimum jet leading charged track p_T cut normalized by the number of entries (see legend). Please note the zero-suppressed y -axis scale.

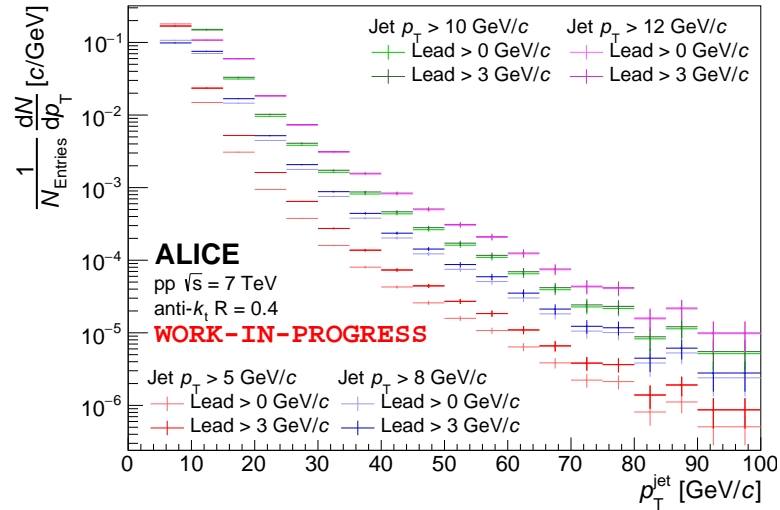
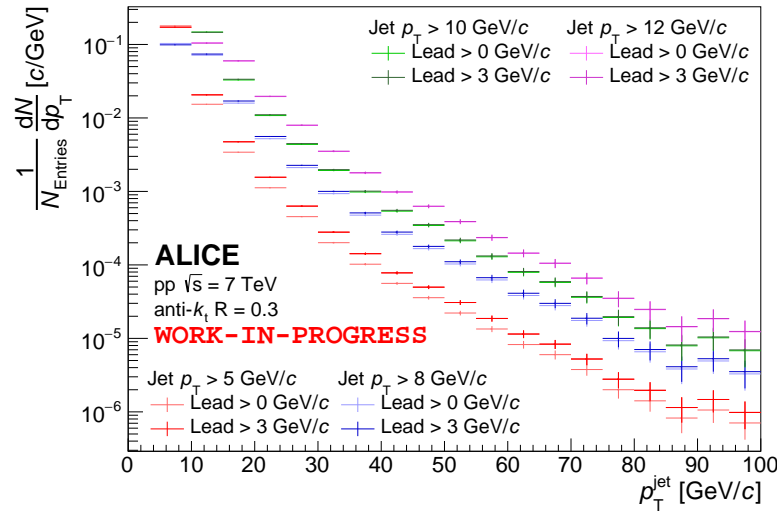
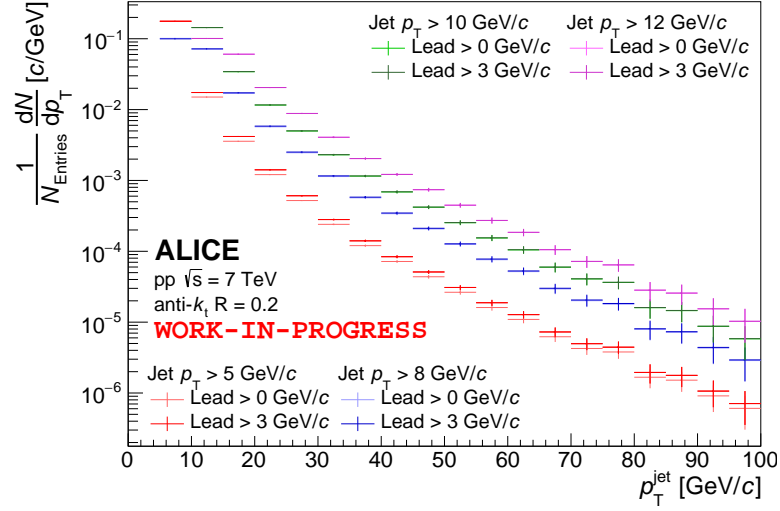


Figure 4.6: p_T -differential spectra of reconstructed inclusive charged jets in pp collisions at $\sqrt{s} = 7$ TeV/c for the three values of the jet resolution parameter $R = 0.2$ (top), 0.3 (middle), 0.4 (bottom) and various combinations of minimum jet p_T and minimum jet leading track p_T cut normalized by the number of entries (see legend).

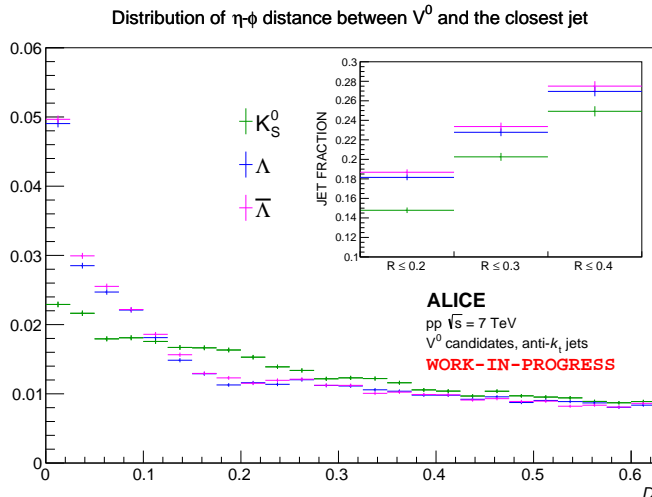


Figure 4.7: Distribution of distance D in $\eta \times \phi$ space between inclusive V^0 candidates and the closest jet axis normalized by the number of entries. In the subframe, the jet fraction (the ratio of jets associated with V^0 and inclusive jets) integrated from $D = 0$ up to $D = R = 0.2, 0.3, 0.4$, respectively, is presented.

4.5 Signal extraction

The V^0 candidates were divided into several groups based of their p_T , then the raw yield extraction was conducted in each p_T region separately by the procedure described in this section. This was done for both cases, the inclusive V^0 candidates and the identified V^0 candidates associated with the charged jets.

First, the invariant mass m_{inv} distribution of V^0 candidates is fitted with sum of Gaussian and linear function representing a signal and a combinatorial background. From result of this approximate fit, values of Gaussian distribution standard deviation σ and mean μ are extracted and used for the estimation of invariant mass limits of peak region and background sidebands, $m^{\text{P}} \in \langle \mu - 6\sigma; \mu + 6\sigma \rangle$ and $m^{\text{BG}} \in \langle \mu - 12\sigma; \mu - 6\sigma \rangle \cup \langle \mu + 6\sigma; \mu + 12\sigma \rangle$, respectively (see Figure 4.11).

Then the invariant mass distribution is fitted with the linear function in the both background sideband regions simultaneously, while excluding the peak region. Since combinatorial background is relatively low in pp collisions in comparison with the Pb-Pb case, there is no need for using different functions for K_S^0 and $\Lambda/\bar{\Lambda}$ background description. Otherwise, using second and higher order polynomial function might improve the quality of the fit, especially in case of $\Lambda/\bar{\Lambda}$ candidates.

Raw yields are obtained via a bin counting method in the peak region, when the signal is estimated simply as a bin content subtracted by the value of fitted background function in the bin centre. The same procedure is also conducted on the m_{inv} distributions of V^0 candidates associated with jets.

Possible alternative for the bin counting method described above is using a combined fit for the background and the signal similarly to the case of the approximated fit. However, since the $\Lambda/\bar{\Lambda}$ peak is very narrow, such a fit is really sensitive to initial values of fit parameters. Also selection of fitting function properly describing the signal is crucial for the signal extraction. Candidate for such a function is a Voigtian function [21], but its

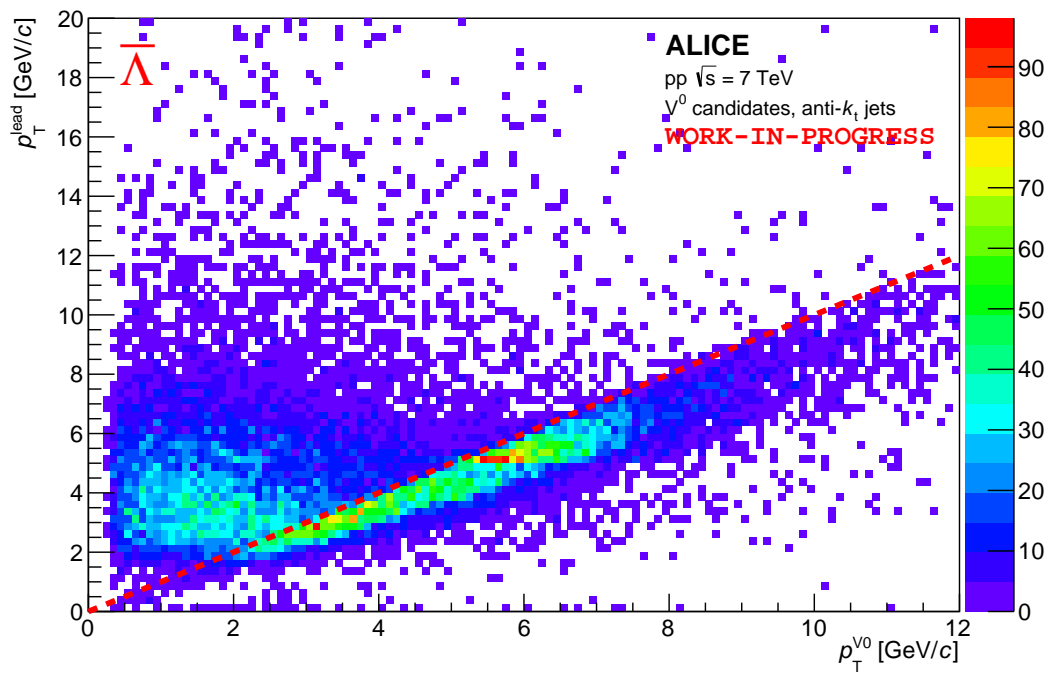
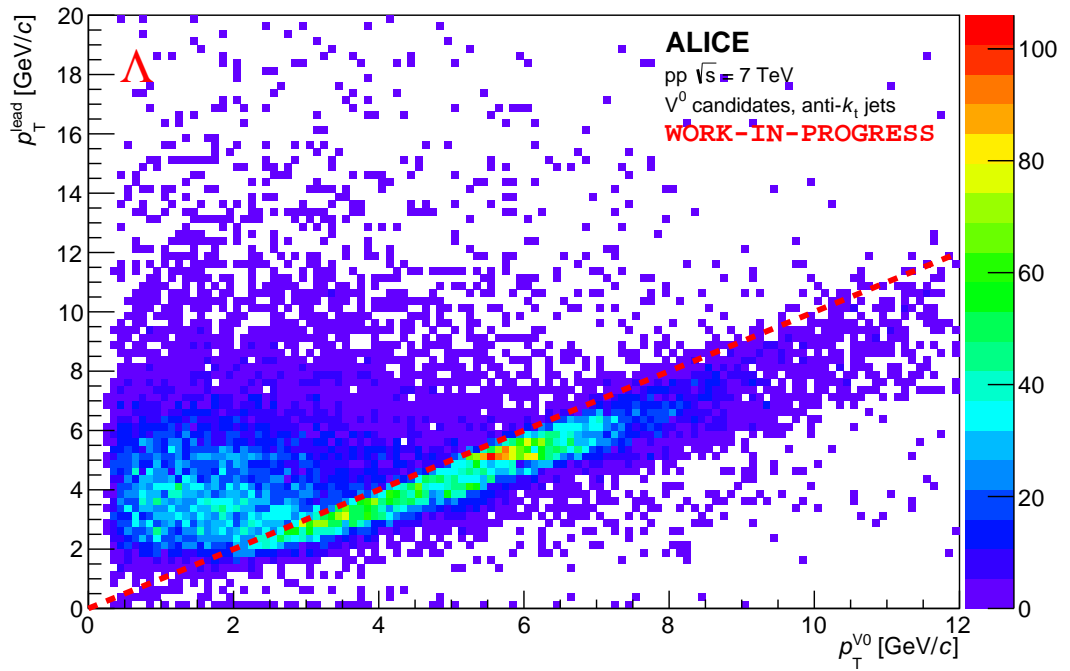


Figure 4.8: Study of the correlation between p_T of V^0 candidates associated with jet and its leading track p_T for Λ (top) and $\bar{\Lambda}$ (bottom) candidates. Red dashed line represents the $x = y$ dependency.

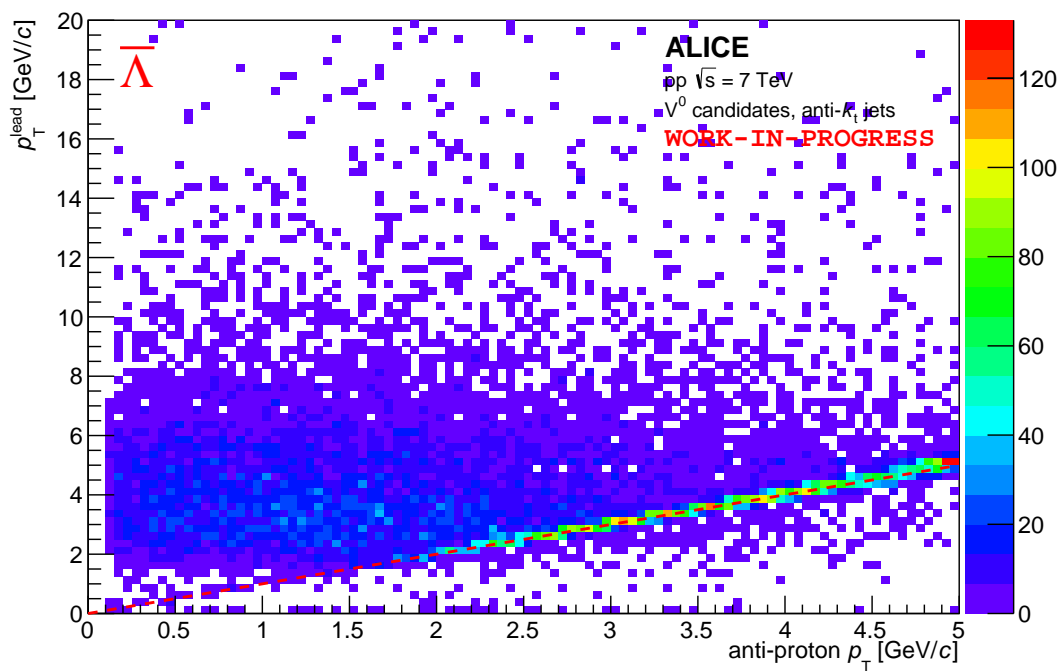
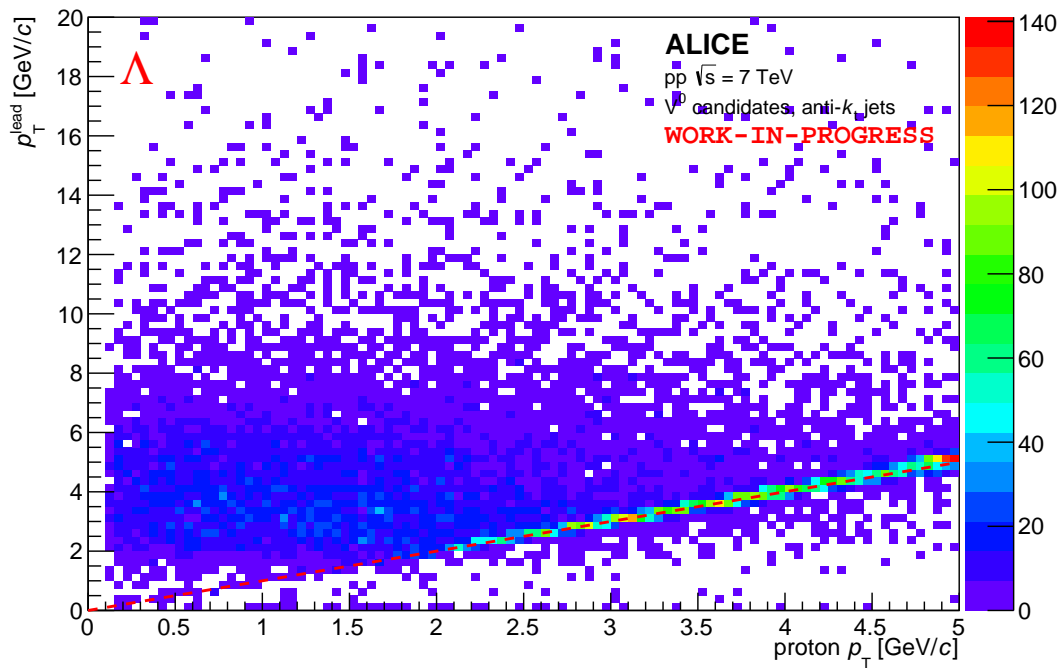


Figure 4.9: Study of the correlation between p_T of proton/anti-proton in Λ (top) / $\bar{\Lambda}$ (bottom) candidates associated with jet and its leading track p_T . Red dashed line represents the $x = y$ dependency.

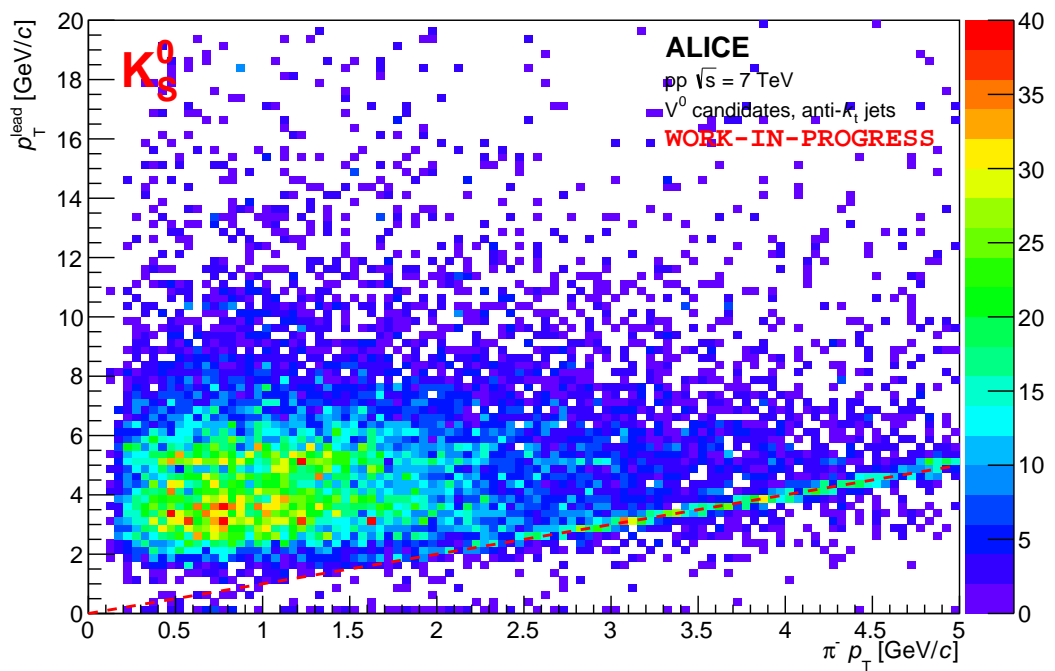
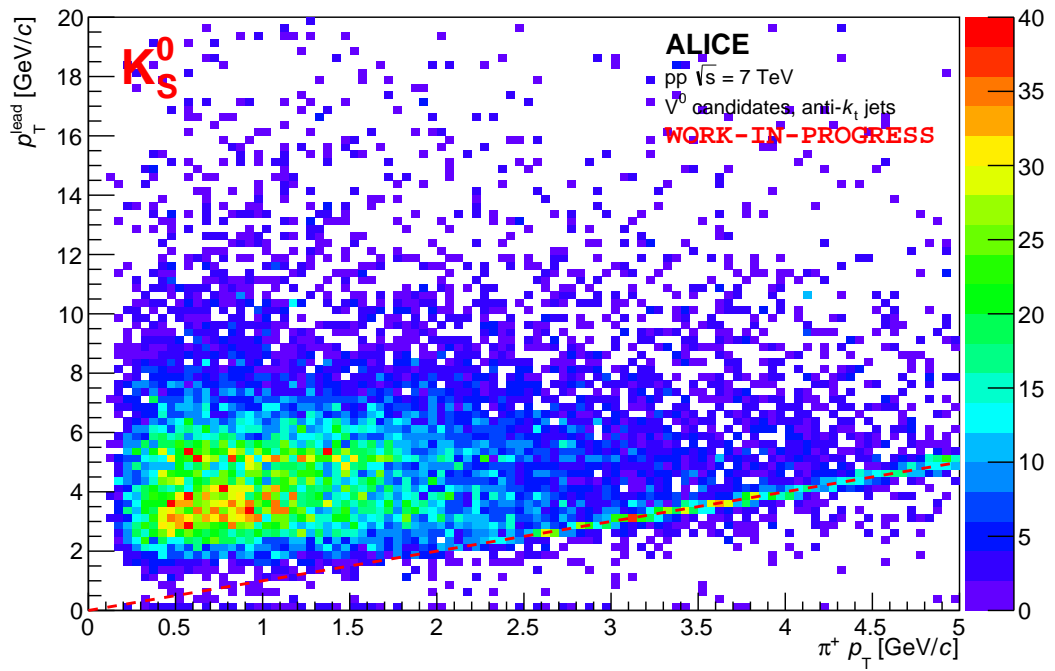


Figure 4.10: Study of the correlation between p_{T} of positive (top) and negative (bottom) pion in K_S^0 candidates associated with jet and its leading track p_{T} . Red dashed line represents the $x = y$ dependency.

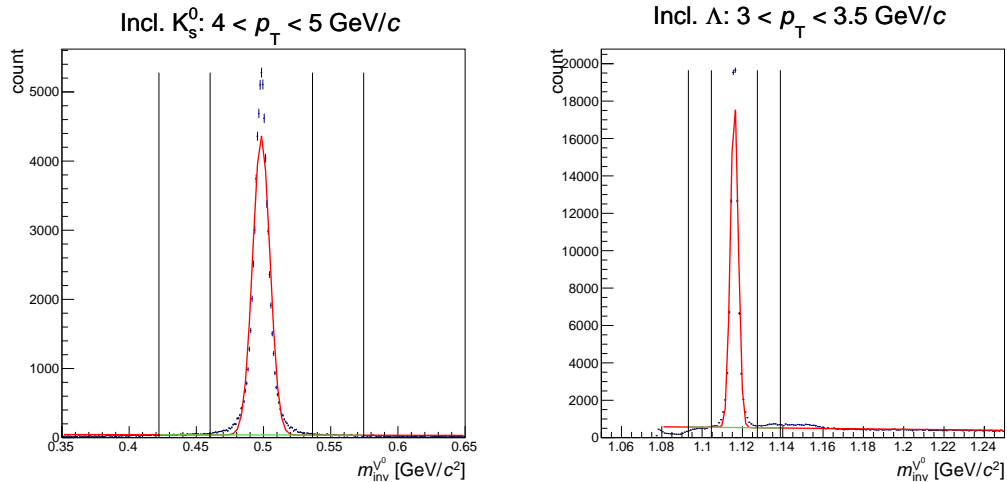


Figure 4.11: Examples of signal extraction method by fitting the invariant mass m_{inv} distribution of inclusive V^0 candidates. The red line indicates the result of approximated fit, black vertical lines correspond to the $\pm 12\sigma$ and $\pm 6\sigma$ boundaries and the green line is a linear function for background estimation in peak region.

current implementation in the ROOT requires a detector resolution as a fitting parameter, which can be obtained by Monte Carlo study only.

4.6 Results

In this section, the results of neutral strange particles analysis of pp collision at $\sqrt{s} = 7$ TeV described in detail in this chapter are presented, both for the inclusive particles and the identified particles associated with charged jets. Please note, that since the systematic uncertainties study has not been done yet, only the statistical uncertainties are included.

4.6.1 Inclusive V^0 particles

The p_T -differential spectra in p_T range from 1 GeV/ c to 12 GeV/ c of the inclusive V^0 particle yields obtained via the signal extraction procedure (described in Section 4.5) applied on the raw inclusive K_S^0 , Λ and $\bar{\Lambda}$ candidates with no additional efficiency correction or feed-down estimation are presented on Figure 4.12.

The ratio of the uncorrected yields of the inclusive neutral strange baryons, Λ to $\bar{\Lambda}$, is presented on Figure 4.13. The resulting $\Lambda/\bar{\Lambda}$ ratio is within 5% consistent with the unity regarding the statistical errors in the whole range of V^0 p_T , except for the last bin probably due to the low statistics. Since the ratio of p/\bar{p} in pp collisions at $\sqrt{s} = 7$ TeV [22] is consistent with unity, this slight deviation (present in other $\Lambda/\bar{\Lambda}$ analyses) is now currently under study within the PWG-LF.

Finally, the ratio of the inclusive neutral strange Λ and $\bar{\Lambda}$ baryons to K_S^0 mesons obtained from the uncorrected yields of V^0 particles is presented on Figure 4.15. It exhibits a similar trend as the results published by the PWG-LF [4] (see Figure 4.14), however the

overall magnitude is higher than the published results. After the proper reconstruction efficiency and $\Lambda/\bar{\Lambda}$ feed-down estimation are applied, more detailed quantitative comparison will be possible.

4.6.2 Identified V^0 particles in charged jets

In this section, the results concerning only the identified V^0 particles associated with charged jets are presented. These jets were reconstructed (see Section 4.4) with the three values of jet resolution parameter $R = 0.2, 0.3, 0.4$ and a various combinations of minimal jet $p_T = 5, 8, 10, 12$ GeV/ c and minimal jet leading charged track $p_T = 0$ and 3 GeV/ c cuts.

The p_T -differential spectra in p_T range from 1 GeV/ c to 12 GeV/ c of the V^0 particle yields obtained from the identified K_S^0 , Λ and $\bar{\Lambda}$ candidates associated with jets in the same way as the inclusive ones with no additional efficiency correction or feed-down estimation are presented on Figures 4.16, 4.17, 4.18, respectively.

The ratio of the uncorrected yields of the identified neutral strange baryons, Λ to $\bar{\Lambda}$, is presented on Figure 4.19. Depending on the chosen combination of the jet selection criteria, consistency with unity is varying. In general, the variance tends to be higher with the increasing value of minimal jet p_T cut and larger value of jet resolution parameter, especially in high V^0 p_T region above 6 GeV/ c .

The ratio of the identified neutral strange Λ and $\bar{\Lambda}$ baryons to K_S^0 mesons associated with reconstructed jets is presented on Figure 4.20. With the loosest jet selection cut of minimal jet $p_T = 5$ GeV/ c , it exhibits a similar trend as the inclusive result, however the maximum is shifted towards the higher V^0 p_T . Even the slight enhancement of Λ and $\bar{\Lambda}$ with respect to K_S^0 is observed in the p_T region around 5 GeV/ c . With the larger value of minimal jet p_T cut, the Λ and $\bar{\Lambda}$ particles are more suppressed, especially in the intermediate V^0 p_T region.

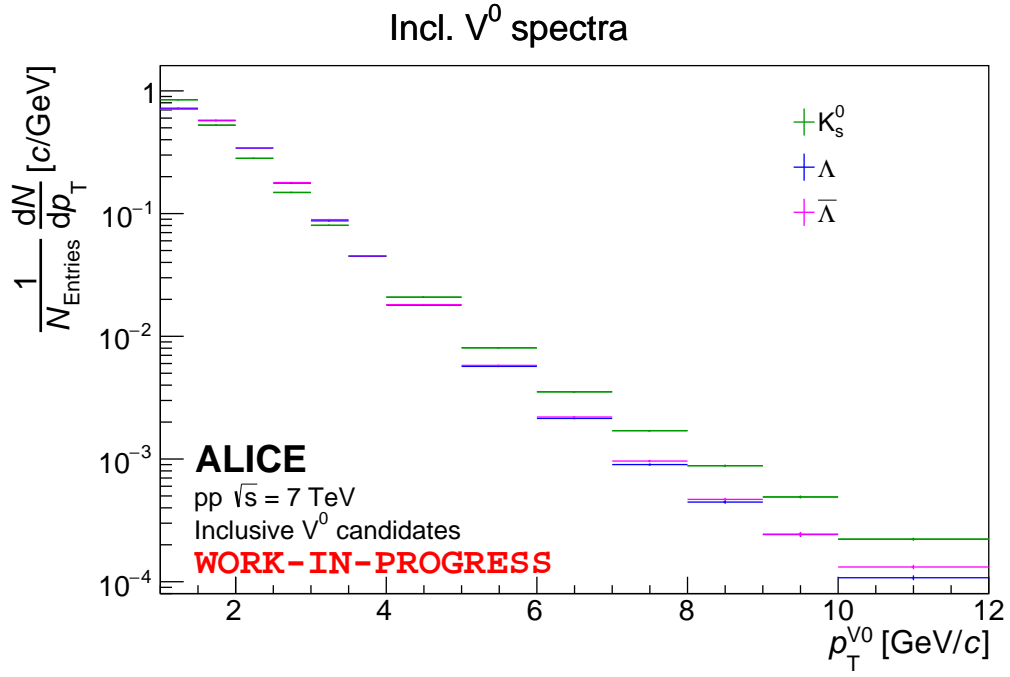


Figure 4.12: Uncorrected p_T -differential spectra of the inclusive K_s^0 , Λ and $\bar{\Lambda}$ after signal extraction procedure.

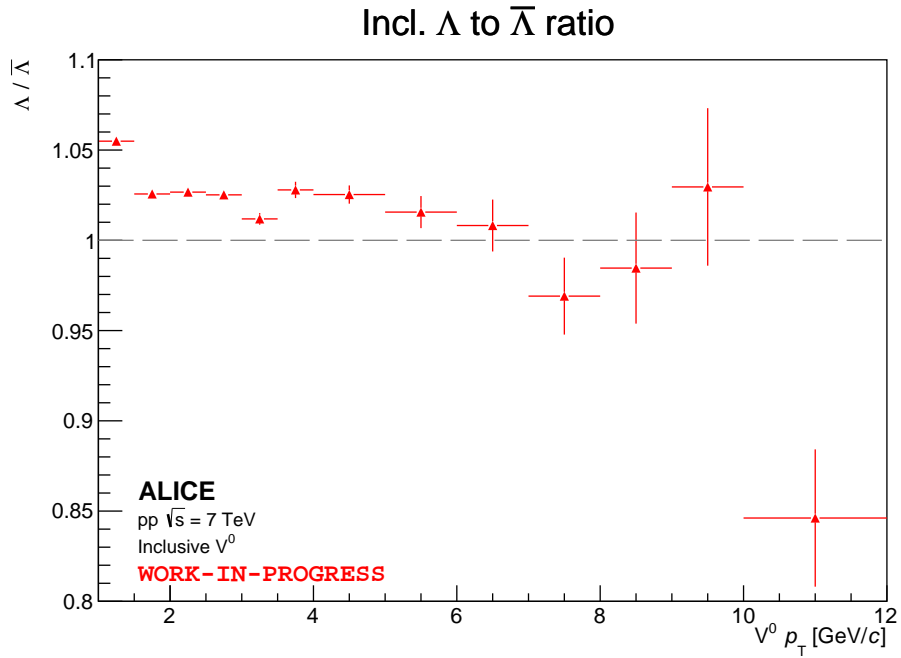


Figure 4.13: Uncorrected p_T -dependent ratio of the inclusive Λ to $\bar{\Lambda}$.

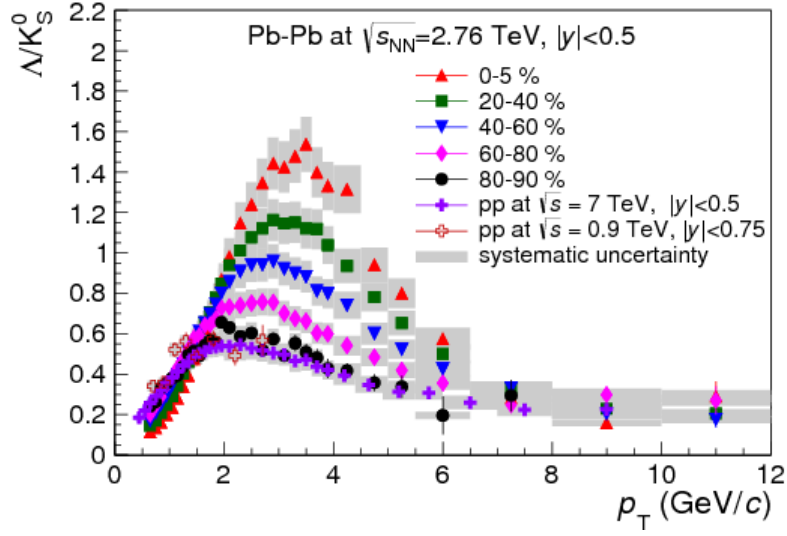


Figure 4.14: Ratio of inclusive production of neutral strange Λ baryons and K_S^0 mesons [4] illustrating the so-called baryon anomaly, the enhancement of baryon production with respect to the meson production in Pb-Pb relative to the pp collisions.

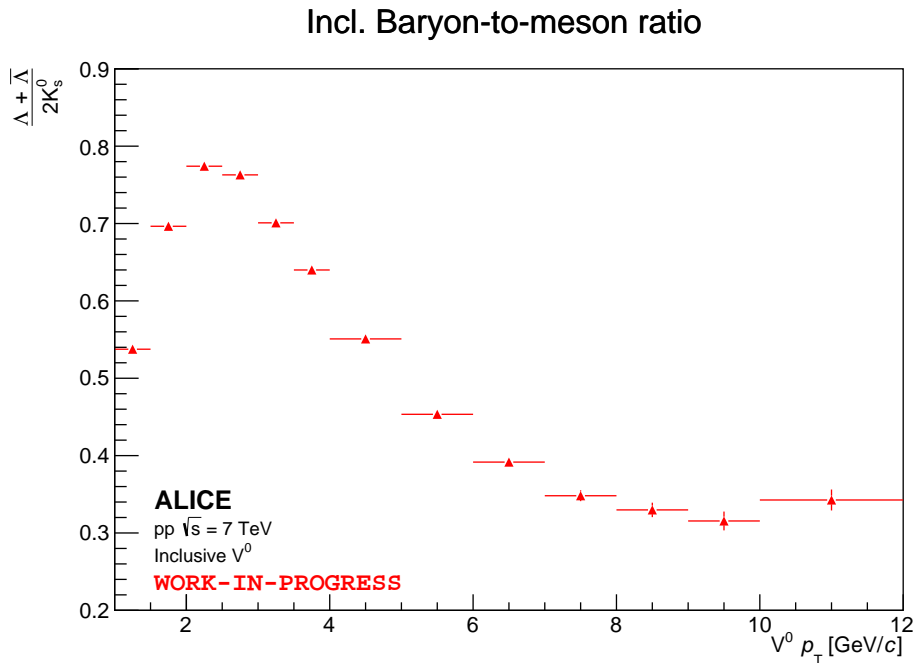


Figure 4.15: Uncorrected p_T -dependent ratio of the inclusive Λ and $\bar{\Lambda}$ to K_S^0 .

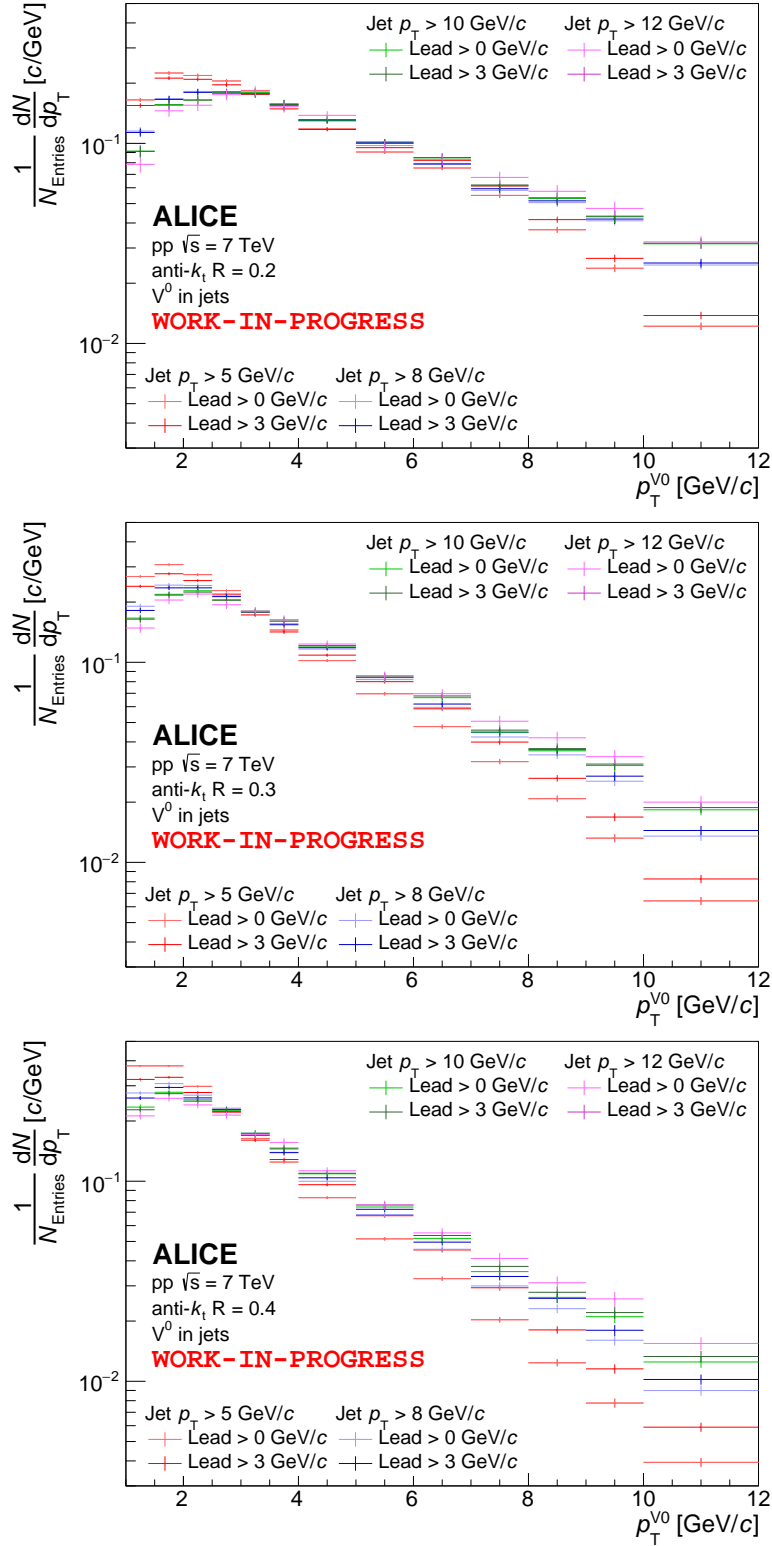


Figure 4.16: Uncorrected p_T -differential spectra of the identified K_S^0 associated with charged jets reconstructed with the three values of jet resolution parameter $R = 0.2$ (top), 0.3 (middle), 0.4 (bottom) and various combinations of minimum jet p_T and minimum jet leading track p_T cut (see legend).

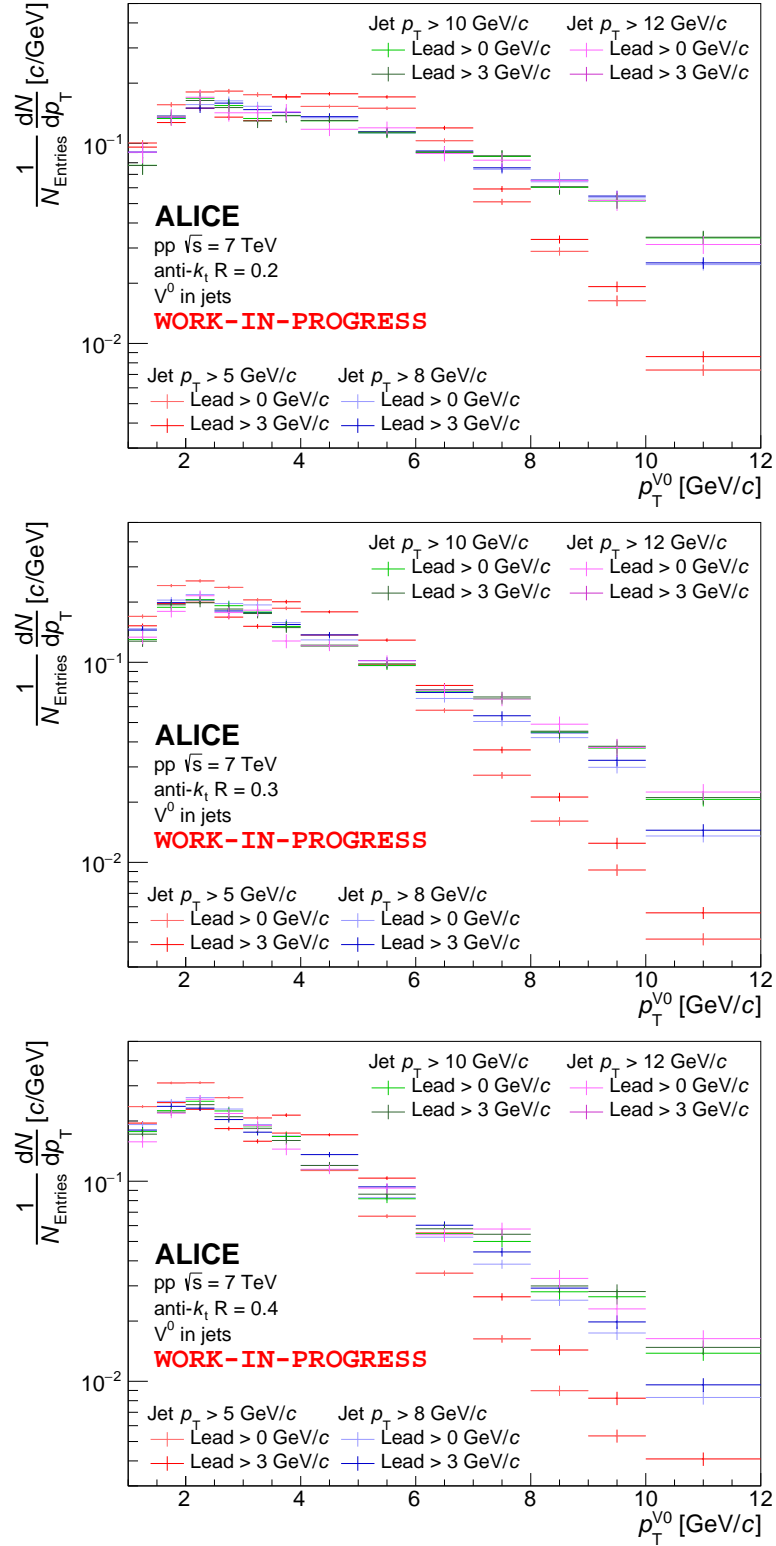


Figure 4.17: Uncorrected p_T -differential spectra of the identified Λ associated with charged jets reconstructed with the three values of jet resolution parameter $R = 0.2$ (top), 0.3 (middle), 0.4 (bottom) and various combinations of minimum jet p_T and minimum jet leading track p_T cut (see legend).

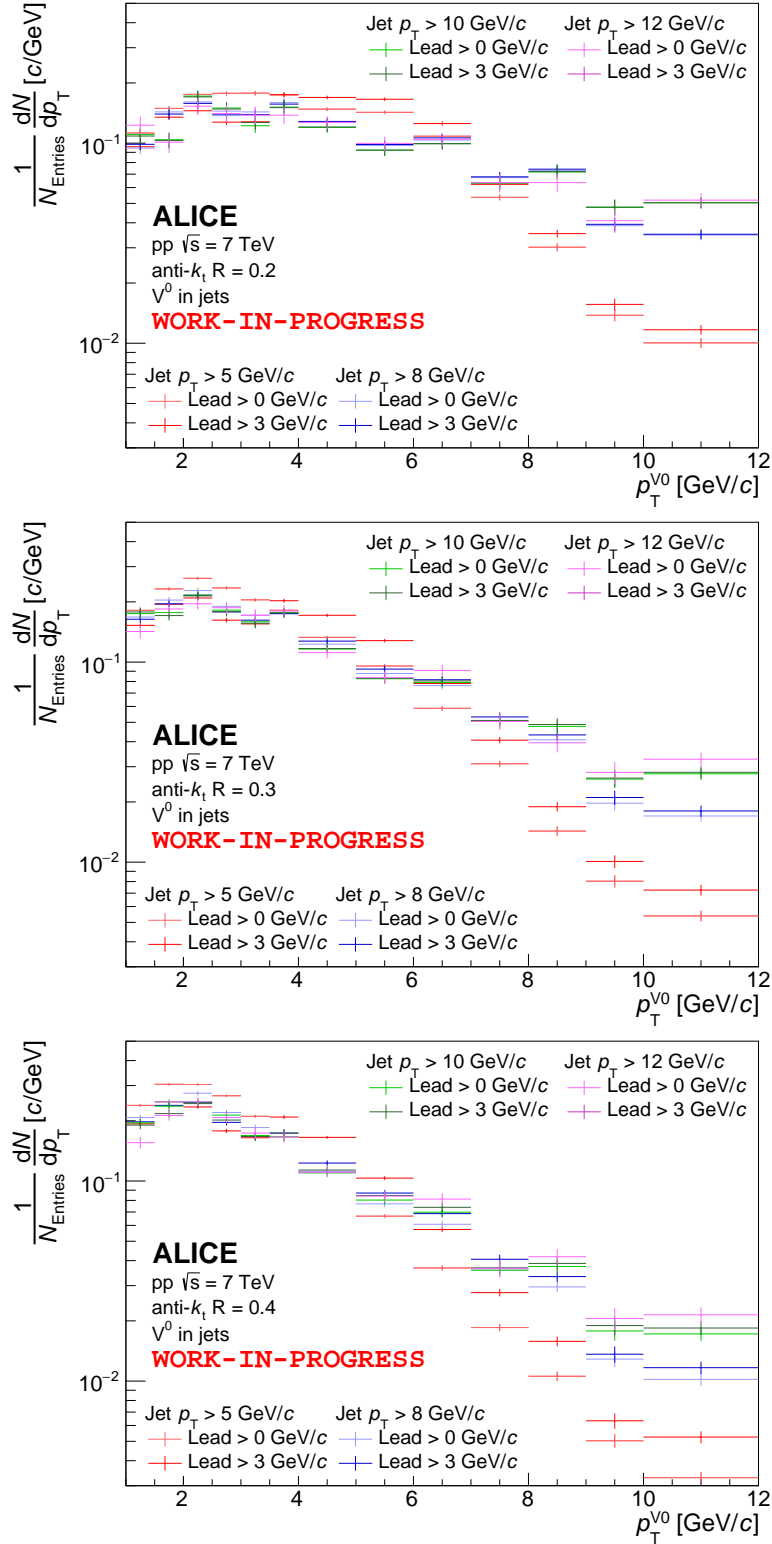


Figure 4.18: Uncorrected p_T -differential spectra of the identified $\bar{\Lambda}$ associated with charged jets reconstructed with the three values of jet resolution parameter $R = 0.2$ (top), 0.3 (middle), 0.4 (bottom) and various combinations of minimum jet p_T and minimum jet leading track p_T cut (see legend).

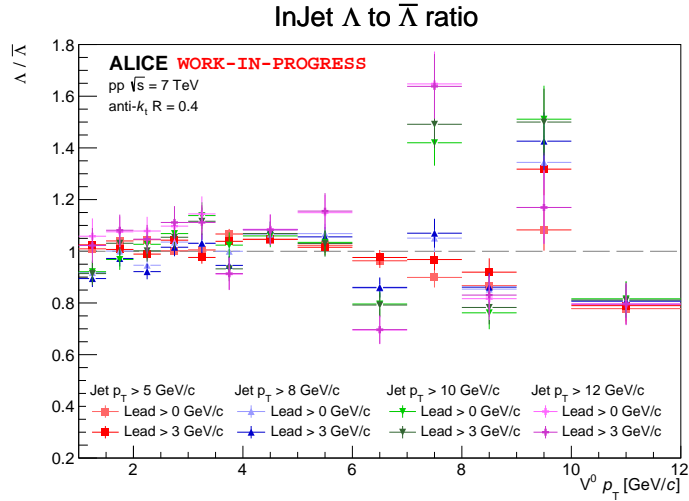
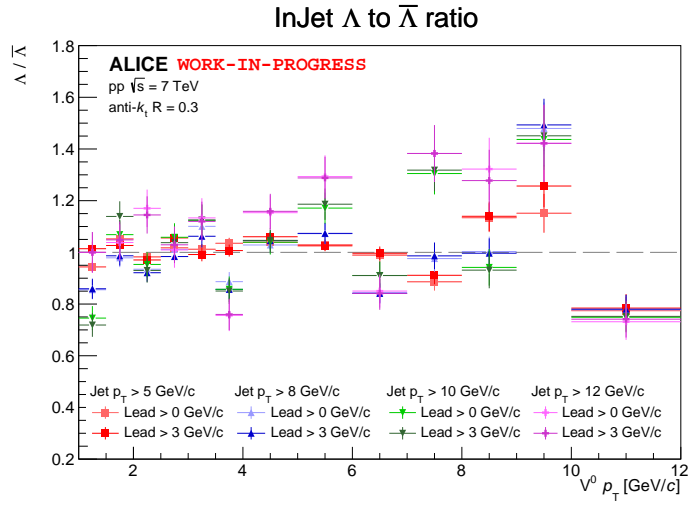
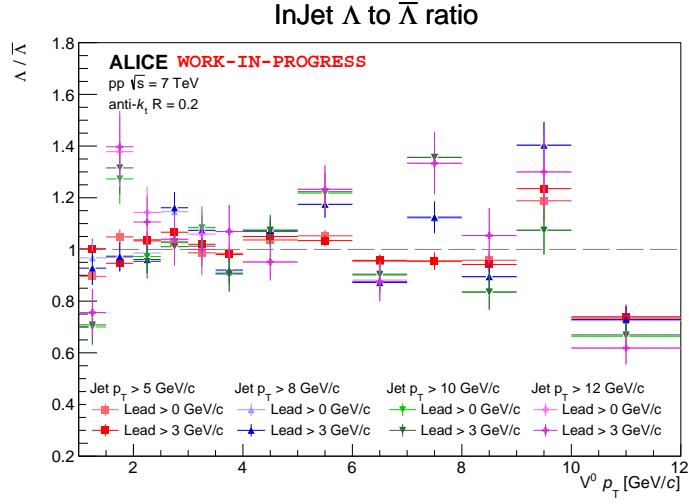


Figure 4.19: Uncorrected p_T -dependent ratio of the identified Λ to $\bar{\Lambda}$ in reconstructed charged jets with the three values of jet resolution parameter $R = 0.2$ (top), 0.3 (middle), 0.4 (bottom) and various combinations of minimum jet p_T and minimum jet leading track p_T cut (see legend).

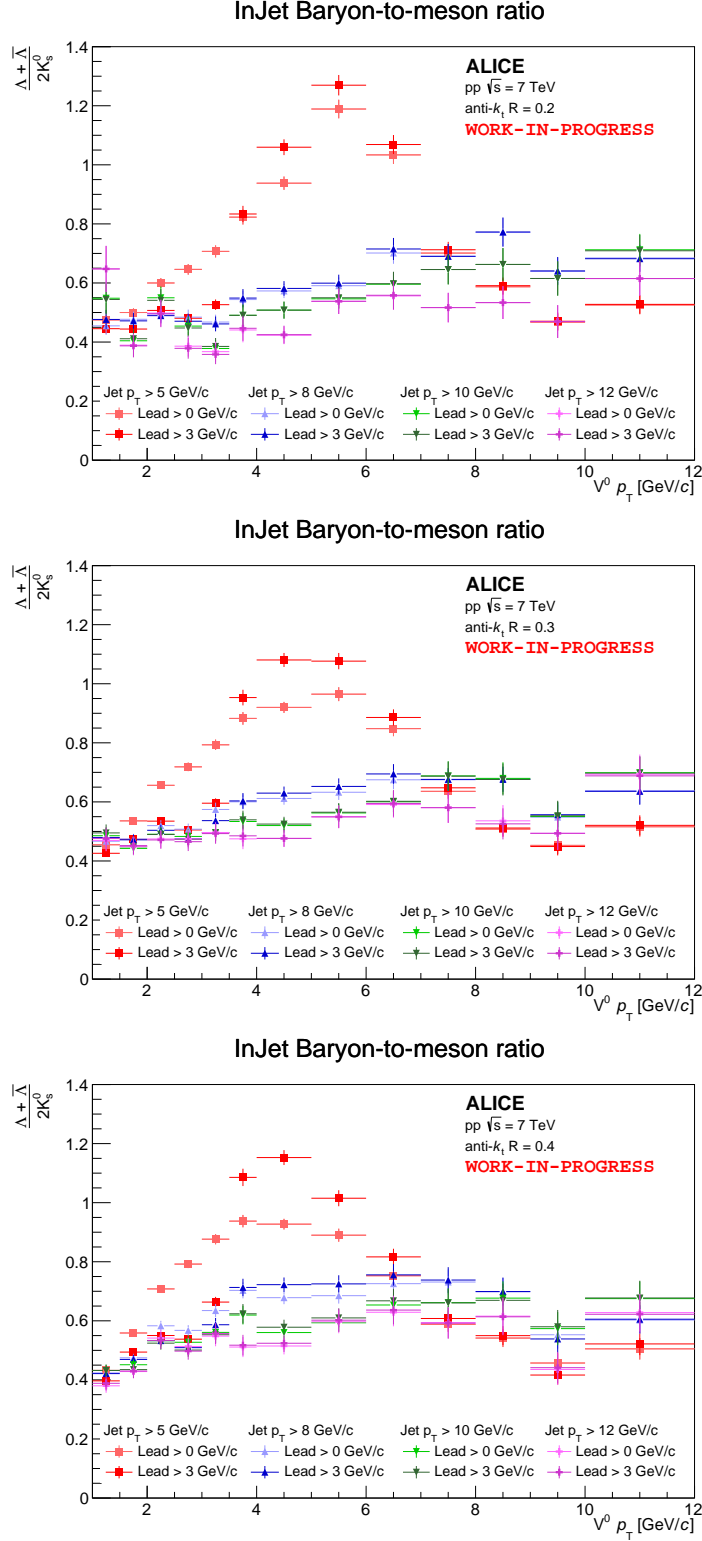


Figure 4.20: An uncorrected p_T -dependent ratio of the identified Λ and $\bar{\Lambda}$ to K_S^0 in reconstructed jets with the three values of jet resolution parameter $R = 0.2$ (top), 0.3 (middle), 0.4 (bottom) and various combinations of minimum jet p_T and minimum jet leading track p_T cut (see legend).

Chapter 5

Summary

Hadron identification in jets plays a crucial role in the theoretical predictions currently under study in the experiments both at the LHC and RHIC and provides a necessary baseline for the studies of proton-nucleus and nucleus-nucleus collisions.

The topological reconstruction and selection of inclusive V^0 particles in p_T range 1 – 12 GeV/ c have been conducted on minimum-bias sample of pp collision at $\sqrt{s} = 7$ TeV measured with the ALICE detector. Analysis of identified K_S^0 , Λ and $\bar{\Lambda}$ associated with charged jets reconstructed with the anti- k_T jet finding algorithm was performed.

The neutral strange baryon-to-meson ratios presented in Section 4.6 exhibit a similar trend as the result published by the PWG-LF, however the magnitude of the ratios are different. This could be caused by the fact, that the presented results are based on the raw V^0 candidate distribution with no reconstruction efficiency correction and no additional feed-down subtraction included. For more detailed comparison with the published data the corrected spectra and ratios, and thus the proper Monte Carlo study, is needed.

In case of the $\Lambda/\bar{\Lambda}$ ratio, the presented uncorrected results of inclusive particles are consistent with unity within approximately 5% in the region of small p_T . In the intermediate V^0 p_T the enhancement of Λ particles appears followed by the steep drop in the higher p_T . The results of the identified $\Lambda/\bar{\Lambda}$ ratio exhibit larger variance with respect to the unity. However this may also change after including the necessary corrections.

The presented spectra of identified K_S^0 , Λ and $\bar{\Lambda}$ associated with jets also display the sensitivity to the jet reconstruction and selection parameters, such as minimum jet leading track p_T (discussed in Section 4.4.1) and minimum jet p_T . The differences between various jet requirements are especially significant in the region of small and intermediate p_T of the selected V^0 particles.

Bibliography

- [1] V. Kučera, *Production of strange particles in charged jets in Pb-Pb and p-Pb collisions measured with ALICE*, *J.Phys.: Conf. Ser.* **612** (2015) 012013.
- [2] **STAR** Collaboration, B. Abelev *et. al.*, *Energy dependence of π^{+-} , p and anti-p transverse momentum spectra for Au+Au collisions at $\sqrt{s_{NN}} = 62.4$ and 200-GeV*, *Phys.Lett.* **B655** (2007) 104–113 [nucl-ex/0703040].
- [3] **STAR** Collaboration, M. Lamont, *Identified particles at large transverse momenta in STAR in Au+Au collisions at $\sqrt{s_{NN}} = 200$ -GeV*, *J.Phys.* **G30** (2004) S963–S968 [nucl-ex/0403059].
- [4] **ALICE** Collaboration, B. B. Abelev *et. al.*, *K_S^0 and Λ production in Pb-Pb collisions at $\sqrt{s_{NN}} = 2.76$ TeV*, *Phys.Rev.Lett.* **111** (2013) 222301 [1307.5530].
- [5] R. J. Fries, B. Muller, C. Nonaka and S. A. Bass, *Hadronization in heavy ion collisions: Recombination and fragmentation of partons*, *Phys. Rev. Lett.* **90** (2003) 202303 [nucl-th/0301087].
- [6] R. J. Fries, V. Greco and P. Sorensen, *Coalescence Models For Hadron Formation From Quark Gluon Plasma*, *Ann. Rev. Nucl. Part. Sci.* **58** (2008) 177–205 [0807.4939].
- [7] D. Molnar and S. A. Voloshin, *Elliptic flow at large transverse momenta from quark coalescence*, *Phys. Rev. Lett.* **91** (2003) 092301 [nucl-th/0302014].
- [8] G. C. Blazey, J. R. Dittmann, S. D. Ellis, V. D. Elvira, K. Frame *et. al.*, *Run II jet physics*, hep-ex/0005012.
- [9] G. P. Salam and G. Soyez, *A Practical Seedless Infrared-Safe Cone jet algorithm*, *JHEP* **05** (2007) 086 [0704.0292].
- [10] J. Tseng and H. Evans, *Sequential recombination algorithm for jet clustering and background subtraction*, *Phys. Rev.* **D88** (2013) 014044 [1304.1025].
- [11] M. Cacciari, G. P. Salam and G. Soyez, *FastJet User Manual*, *Eur.Phys.J.* **C72** (2012) 1896 [1111.6097].
- [12] M. Cacciari and G. P. Salam, *Dispelling the N^3 myth for the k_T jet-finder*, *Phys.Lett.* **B641** (2006) 57–61 [hep-ph/0512210].
- [13] M. Cacciari, G. P. Salam and G. Soyez, *The Anti- k_T jet clustering algorithm*, *JHEP* **0804** (2008) 063 [0802.1189].
- [14] Y. L. Dokshitzer, G. D. Leder, S. Moretti and B. R. Webber, *Better jet clustering algorithms*, *JHEP* **08** (1997) 001 [hep-ph/9707323].

- [15] **ALICE** Collaboration, K. Aamodt *et. al.*, *The ALICE experiment at the CERN LHC, JINST* **3** (2008) S08002.
- [16] **Particle Data Group** Collaboration, K. A. Olive *et. al.*, *Review of Particle Physics, Chin. Phys.* **C38** (2014) 090001.
- [17] V. Kučera and A. Zimmermann, *Production of K_S^0 , Λ and $\bar{\Lambda}$ particles in charged jets in Pb-Pb collisions at $\sqrt{s_{NN}} = 2.76$ TeV measured with ALICE, ALICE Analysis Note.*
- [18] Chinellato, D. David, *K_S^0 , Λ and $\bar{\Lambda}$ production in proton-proton collisions at $\sqrt{s_{NN}} = 7$ TeV, ALICE Analysis Note.*
- [19] “Introduction: Hybrid tracks.”
- [20] M. Cacciari, G. P. Salam and G. Soyez, *FastJet User Manual, Eur. Phys. J.* **C72** (2012) 1896 [1111.6097].
- [21] R. C. Baral, *Signal of Λ (1520) baryon resonance in pp collisions at $\sqrt{s_{NN}} = 7$ TeV, ALICE Analysis Note.*
- [22] **ALICE** Collaboration, K. Aamodt *et. al.*, *Midrapidity antiproton-to-proton ratio in pp collisions at $\sqrt{s} = 0.9$ and 7 TeV measured by the ALICE experiment, Phys. Rev. Lett.* **105** (2010) 072002 [1006.5432].